25

IS-T--1836

RHEED Studies of Vicinal Si(111) Surfaces and Ag Films Grown on Si(111)

by

Stanley, Michael Kevin

PHD Thesis submitted to Iowa State University

Ames Laboratory, U.S. DOE
Iowa State University
Ames, Iowa 50011

Date Transmitted: February 23, 1998

PREPARED FOR THE U.S. DEPARTMENT OF ENERGY
UNDER CONTRACT NO. W-7405-Eng-82.

DISCLAIMER

This report has been reproduced directly from the best available copy.

AVAILABILITY:

To DOE and DOE contractors: Office of Scientific and Technical Information
P.O. Box 62
Oak Ridge, TN 37831

prices available from: (615) 576-8401
FTS: 626-8401

To the public: National Technical Information Service
U.S. Department of Commerce
5285 Port Royal Road
Springfield, VA 22161

RHEED studies of vicinal Si(111) surfaces and Ag films grown on Si(111)

Michael Kevin Stanley

Major Professor: Michael C. Tringides

Iowa State University

Reflection high energy electron diffraction (RHEED) was used to study the growth of silver films and the evolution of step structures on the silicon (111) surface. Silver films were deposited by molecular beam epitaxy onto the Si(111) 7 x 7 surface. Films deposited below room temperature showed RHEED intensity oscillation whose quality improved with decreasing temperature. RHEED oscillations were also improved by the application of an initial burst in the deposition flux. Such improvement and the temperature dependence of the oscillations is attributed to an increase in the island nucleation density.

Vicinal silicon samples miscut from the (111) plane by 1.2°, 2.5°, and 4.5° towards the $[2\bar{1}\bar{1}]$ direction were studied. If the samples were cooled slowly through the 1 x 1 to 7 x 7 phase transition a step bunching transformation would occur that produced large (111) terraces. During this transition the diffraction spot splitting would vanish while maintaining a constant splitting width. This suggest that the transition occurs by the growth of a few terraces incorporating the others with the widths of the other terraces remaining fixed until incorporation.

TABLE OF CONTENTS

ACKNOWLEDGMENTS

I never could have completed this work and my formal education without the support, in various forms, of an enormous number of people. I wish to thank my parents, Marland and Rachel Stanley, for the support that they provided, both moral and financial, at various times. I also wish to thank those who befriended me during my studies, many of whom came and went, but without whom I certainly would not have completed my degree.

It is necessary to acknowledge my major professor, Michael C. Tringides, who has played a major role in shaping my future. I also wish to express my appreciation to the other members of my committee and those who substituted in their absence, Professors James Evans, Bruce N. Harmon, David W. Lynch, Steven Kawaler, Jianwei Qui, and Andrew E. DePristo. I thank them for their time, consideration, and the corrections and suggestions which some of them made that improved the quality of this manuscript. I would also like to thank Professor D. K. Finnemore for listening when I needed to talk and providing words of encouragement at a critical time.

This work was performed at Ames Laboratory under Contract No. W-7405-Eng-82 with the U.S. Department of Energy. The United States government has assigned the DOE Report number IS-T 1836 to this thesis.

1. GENERAL BACKGROUND

1.1 Introduction

The study of surfaces has yielded a considerable amount of interesting information, some of which has found practical application. However, much is still unknown about many surfaces and their growth. This thesis describes experiments that were performed to examine the growth of silver on silicon and the evolution of step structures on vicinal silicon surfaces. Silicon surfaces have been among of the most widely studied as a consequence of silicon's importance to the semiconductor industry. Even for basic surface research, silicon is often chosen over other materials because it is economically available in high purity crystals conveniently precut into wafers. This along with the value of the experience already possessed by the research group in which the author studied motivated its choice for these experiments. Silver was chosen for the growth studies because it does not significantly intermix with silicon and could be readily removed to allow reuse of the samples.

Like many other covalently bonded crystals, the surfaces of silicon will form reconstructions that can differ significantly from their bulk terminations. In the bulk, (111) planes of silicon consist of a bilayer of atoms with the plane in which half the atoms are located displaced from the plane that contains the other half by 0.77 Å. The spacing between adjacent (111) bilayers is 3.1 Å. Below approximately 850°C the (111) surface of silicon reconstructs into a 7 x 7 formation three atomic bilayers deep. This 7 x

7 reconstruction is an equilibrium shape, and it is possible to quench in the 1 x 1 formation that exists at higher temperatures by cooling the sample back down quickly after heating. When silver is deposited onto the 7 x 7 Si (111) surface it can form a number of temperature-dependent superstructures [1]. In this work only experiments in the temperature range where the deposited silver forms as layers of the (111) plane of the silver face-centered cubic crystal will be discussed.

A great many experimental techniques are available for the study of surfaces. Among them, reflection high-energy electron diffraction (RHEED) is particularly attractive for studying film growth. In its simplest form a RHEED apparatus consists of an electron gun positioned for a glancing incidence angle and a phosphor screen to observe the diffraction pattern on the opposite side of the sample. The advantage of this set up is that no equipment is positioned directly over the sample where it could interfere with film deposition. This allows film growth to be monitored in real time without the need for the deposition to be temporarily suspended while the sample is repositioned for observation, as must be done with many other techniques.

Using RHEED, information about surface evolution may be obtained by observing changes in the shapes or intensities of the diffraction spots. A common observation during the deposition of many films is the appearance of oscillations in the intensity of the specularly diffracted spot with periods approximately equal to the monolayer completion times of the growing films. Such oscillations are depicted in Figure 1.1 for the growth of silver on silicon (111) at 170K. This has been interpreted as a consequence of these films growing in a layer-by-layer fashion. A simple, but not necessarily complete and accurate, explanation for these oscillations is that they are due to periodic changes in the interference of the reflections from the growing level and the partially exposed completed level just beneath it.

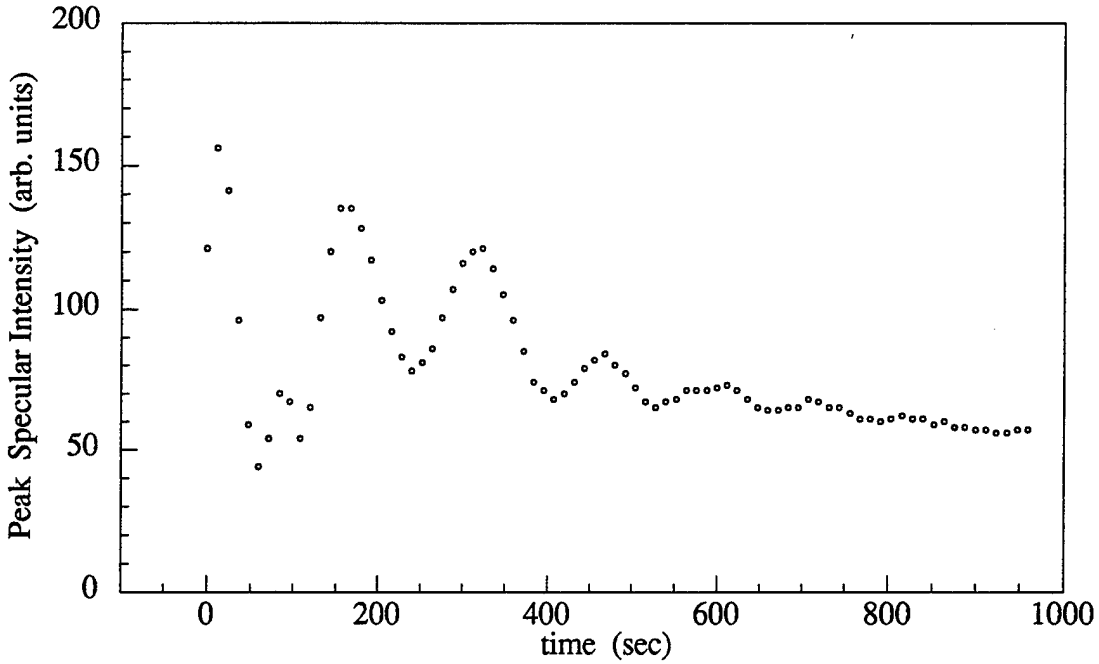

Figure 1.1 Damped oscillations of the peak intensity of the specular beam are shown for silver grown on the Si(111) 7 x 7 surface at 170K.

1.2 Film Growth

When a film is grown on an initially clean, flat surface the first arriving atoms will migrate randomly across the surface until some critical number of them meet and nucleate to form an island of what will become the first overlayer. A number of islands will form in this manner. After this point different modes of growth are possible. If the film grows in a layer-by-layer fashion, sometimes called Frank-van der Merwe growth, these islands will grow and coalesce to complete the layer before the next layer is started. This process repeats itself as each layer of the film is deposited, and the result is a smooth

film which will display RHEED oscillations. Another possibility is Volmer-Weber growth. This is a three dimensional growth mode where the initially nucleated islands grow to be mounds several atomic levels high, and a layer is completed only when the bases of all the mounds have met. This type of growth produces a monotonic decay in the intensity of the specularly diffracted beam. A third case, Stranski-Krastanov growth, involves completion of the first layer in a layer-by-layer fashion followed by 3D growth on top of the initial layer. The growth modes just described are somewhat idealized. Layer by layer growth observed experimentally always has at least some 3D characteristics.

For layer-by-layer growth to occur atoms that arrive on top of an existing island must migrate to the island's edge and descend. However, RHEED intensity oscillations have been observed at temperatures as low as 16K [2]. This has prompted the proposal of various nonthermal transport mechanisms to explain the adatom mobility apparently necessary for layer-by-layer growth. One interesting proposal is that the latent heat of condensation of the atoms arriving from the gas phase is transformed into kinetic energy of the newly arrived atoms giving them a transient mobility until this energy is thermalized by the lattice. Some evidence against this proposal exists, and the matter is currently somewhat controversial. Sanders and DePristo [3] have performed simulations which show a lack of transient mobility for Cu (001) surfaces during homo-epitaxy at 80K suggesting that the RHEED oscillations reported by Egelhoff and Jacob [4] for such an experiment were not caused by transient mobility induced layer-by-layer growth. Evans et al. [5] have proposed another nonthermal mechanism for the growth of fcc (100) surfaces. They propose that at low temperatures arriving atoms are in effect transported parallel to the surface by a "downward funneling" action of atoms arriving on the sides of pyramid shaped structures on the surface. They further point out that RHEED intensity oscillations are not necessarily due to true layer-by-layer growth, but could be caused by

the cyclic evolution of structures capable of downward funneling. Such nonthermal growth mechanisms are not required to explain all the observations of RHEED oscillations as they have been seen at elevated temperatures and also in systems with diffusion barriers so small that thermal diffusion may operate well below room temperature.

The number of islands that nucleate on the initial surface will be an important factor in determining the type of growth for a given film. This number may be affected by the rate at which atoms are deposited and the temperature of the surface as well as other factors that are harder to control such as the concentration of surface defects. Surface defects may act as sites which trap arriving atoms. Point defects may act as island nucleation centers, and extended defects such as steps may trap all arriving atoms before any islands can nucleate, drastically affecting the growth mode. The common theory of nucleation, reviewed by Venables et al. [6,7], predicts that the island density will be proportional to some power of the ratio of the deposition flux to the rate of surface diffusion. For the case of irreversible island growth where all islands larger than a certain size, i, are considered stable, the island density, N, is predicted to obey the relation

$$N \propto \left(\frac{F}{D}\right)^{i/(i+2)} \tag{1.1}$$

where F and D are the rate of arriving atoms and surface diffusion rate respectively. This equation assumes that the rate of surface evaporation is negligible so should be applicable at sufficiently low temperatures or in cases where atoms quickly attach to existing islands. In the absence of defects, the smallest exponent possible in this equation is 1/3, corresponding to the case where all islands larger than a single adatom are stable against disassociation. However, experimentally smaller values of this exponent have been found or even an independence of the island density on the flux rate (an exponent of

zero). The presence of defects can result in a critical cluster size of zero, and is one possible explanation for the small values of this exponent determined from experiment.

K. Roos [8], who previously studied with the author's advisor and to whom the author is indebted for assembling the vacuum chamber used in these studies, found the evolution of the specularly diffracted beam to be independent of the deposition flux rate during the deposition of silver on the Si(111) 7 x 7 surface. Since at low temperature decaying RHEED oscillations were observed whose quality may reasonably be expected to depend on the island density, this may seem to contradict equation 1.2.1. However, it is questionable in this case that the requirement of irreversible island growth is met. After the first layer of silver has been deposited this condition is even less likely to be satisfied during the growth of future layers. Jones et al. [9] have shown the pair-binding energies for Ag dimers and trimers on a two monolayer thick Ag(111) intermediate layer deposited on W(110) to be near 0.3 eV. It seems reasonable that once the silicon surface is covered with silver that the energy required for silver to detach from island edges is also low, and that the rate at which atoms break away from the islands is significant. Also, although reported to be independent of flux, the evolution of the specular beam may have a weak flux dependence. In an experiment described later, a burst of initial flux was seen to enhance nucleation in the initial layer of the silver film indicating a flux dependence of the island density.

The shape of the islands may also have an important influence on growth. Good interlayer transport is critical for layer-by-layer growth, and dendritic shaped islands will favor this since atoms arriving on top of them are more likely to diffuse to and over an edge before meeting other adatoms and nucleating a new layer. Dendritic islands are more likely to form at lower temperatures where the edge diffusion barrier can not be overcome and atoms which attach to an island may then be immobile, while at higher temperatures attaching atoms might diffuse around the island's edge coming to rest where

they find more nearest neighbors to produce smoother islands. It is widely accepted that an additional barrier to diffusion exists for atoms to cross a step edge, and plausible that such a barrier might be reduced at kinks. This factor would also increase interlayer transport in the presence of dendritic shaped islands.

1.3 Vicinal Surfaces

By cutting a crystal slightly off a low-index plane a surface which is a series of terraces separated by single-height atomic steps may be created. Since this will not necessarily be an equilibrium structure it should not be surprising that, given the required energy, such a vicinal surface will often facet into larger terraces of the low index and intervening surfaces of another orientation. Vicinal surfaces are also of interest because of the effect the steps have on growth. The most notable example is the case of step flow, where deposited atoms migrate to the step edges and attach without the formation of islands on the terraces. Step flow results in diffraction spots of constant intensity and shape as the surface is in a steady state.

Silicon surfaces miscut slightly from the (111) plane show a number of interesting features. Except for a few possibilities, such as current-induced step bunching discussed in the next paragraph, the surface will display uniform terraces separated by single atomic steps above the 7 x 7 to 1 x 1 phase transition. Below this transition various forms of step bunching have been reported by different authors, often depending on the direction of the miscut. The temperature at which the 1 x 1 to 7 x 7 transition occurs has even been reported to be a function of the miscut cut angle for surfaces miscut towards the $[1\bar{1}0]$ direction [10]. For samples miscut towards the $[1\bar{1}0]$, $[\bar{1}\bar{1}0]$, and $[\bar{2}11]$ directions the creation of large (111) terraces has been reported [11-13]. There is some discrepancy in the literature about this, though, for surfaces miscut towards the $[\bar{2}11]$. For the $[\bar{2}11]$ and

[$2\bar{1}\bar{1}$] miscuts, small quantities of impurities have been reported to alter significantly the step configuration [13].

Vicinal silicon (111) surfaces that are heated by direct current have been observed to form bands with a high density of steps separated by regions of low step density at certain temperatures [14-17]. Unlike the step bunching described in the previous paragraph, this happens at temperatures that do not correspond to phase transitions of the surface reconstruction, and is a consequence of the current flowing through the sample. The temperature at which this step bunching occurs depends on the direction of the applied current, and this transition is reversible. Latyshev et al. [14,15] report that this step bunching occurs in the range 1050-1250°C and again above 1350°C when current flows in the step-up direction. For current in the step-down direction they report step bunching occurring between 1250-1350°C. These authors also reported that they were unable to observe any such step bunching when an alternating current was used to heat the sample.

This thesis discusses Si(111) surfaces miscut towards the [$2\bar{1}\bar{1}$]. For this miscut direction, a tripling of the step height with no faceting has been reported by Phaneuf and Williams [18] for samples miscut by 6° and 12° and also by Olshanetsky and Teys [13] for a miscut of 8°. Jentzsch and Henzler [19], however, report observing a mixture of step heights on their sample miscut by 16° towards the [$\bar{2}11$]. Phaneuf and Williams have also [18] reported that the temperature at which the 1 x 1 to 7 x 7 transition occurs is independent of the miscut angle for this miscut direction. That surfaces miscut towards the [$\bar{2}11$] and [$2\bar{1}\bar{1}$] directions have such different results reported for them may at first seem strange until it is considered that the bulk termination of their step edges have a different number of dangling bonds. Step edges of surfaces miscut towards the [$2\bar{1}\bar{1}$] have two dangling bonds per atom while those of surfaces miscut towards the [$\bar{2}11$] have only one.

1.4 Spot Profile Analysis

In surface diffraction experiments the positions of the diffraction spots can give the same kind of information about atomic separation and periodicity as in bulk diffraction. RHEED can be used in this manner. However, if this is all the information sought other techniques, such as low energy electron diffraction (LEED), may be better suited because of complications caused by the typical RHEED geometry. RHEED can be used to extract statistical information about island or step positioning, and is well suited for this role because of its high resolution in one direction and a long coherence length or transfer width. This kind of statistical information is obtained from an analysis of the diffraction spot shapes, usually by looking at spot profiles along the high resolution direction.

For bulk diffraction the concepts of a reciprocal lattice and Ewald sphere allow visualization or graphical portrayal of the position of diffraction spots. For surface diffraction, the shapes of the spots may be understood in this fashion as well. The bulk definition of a reciprocal lattice vector, $\mathbf{b}_i$, is given by

$$\mathbf{b}_i = 2\pi \frac{\mathbf{a}_j \times \mathbf{a}_k}{\mathbf{a}_i \bullet \mathbf{a}_j \times \mathbf{a}_k} \tag{1.2}$$

where $\mathbf{a}_i$,, $\mathbf{a}_j$, and $\mathbf{a}_k$ are the real space lattice vectors. This definition may be used for surfaces as well so long as the third real space vector is taken as perpendicular to the surface. This leads to the reciprocal lattice of a flat surface being a series of infinite rods running perpendicular to the surface. These rods, though often depicted as solid objects, are graphical representations of three dimensional functions. When depicted in this manner the rods are actually surfaces which enclose portions of reciprocal space where these functions differ significantly from zero. The fewer the number of scatterers that lead to creation of a certain rod the broader it will be.

After the reciprocal lattice has been constructed the Ewald construction may be used. This is done by constructing a sphere in reciprocal space which intersects the base of a reciprocal rod with a radius drawn to this point that is the wavevector of the incident beam. Where the reciprocal lattice intersects the Ewald sphere corresponds to the appearance of diffraction spots. Figure 1.2 shows the Ewald construction for both LEED and RHEED geometries. Note that in the case of RHEED the diffraction pattern is obtained by extending the allowed beams, those determined to exist by the Ewald sphere-reciprocal lattice intersection, from the center of the Ewald sphere to a plane representing the flat screen on which the pattern is viewed. This pattern is approximately the same as the projection of the reciprocal lattice-Ewald sphere intersection onto the phosphor screen. This causes the spots of the RHEED diffraction pattern to be arranged in a series of arcs. Part (c) of figure 1.2 shows the Ewald sphere viewed from the direction of the screen. It also depicts the arcs seen in the diffraction pattern with one arc containing the $0\bar{1}$, 00, and 01 spots and the rest of the spots shown forming a second arc. The numbers identifying a particular spot are derived from the coordinates (in units of reciprocal lattice vectors) of the reciprocal lattice rod responsible for the corresponding spot. The origin of this coordinate system is placed at the location of the rod to which the incident wavevector was drawn in the Ewald construction, and as with the system of Miller indices, negative numbers are represented by the presence of a bar over that number. Using this convention the specularly diffracted beam creates the 00 spot.

The reciprocal lattice rods will be uniform only if the surface is perfectly flat. Multilevel surfaces will lead to lattice rods that have texture, and the shape of each diffraction spot will be that cross-section of the corresponding rod which intersects the Ewald sphere. Reciprocal lattice rods of multiple level surfaces will have modulations in their diameters with periods of 2π times the inverse of the layer separation. The in and out-of-phase conditions for a given spot will occur when the Ewald sphere intersects its

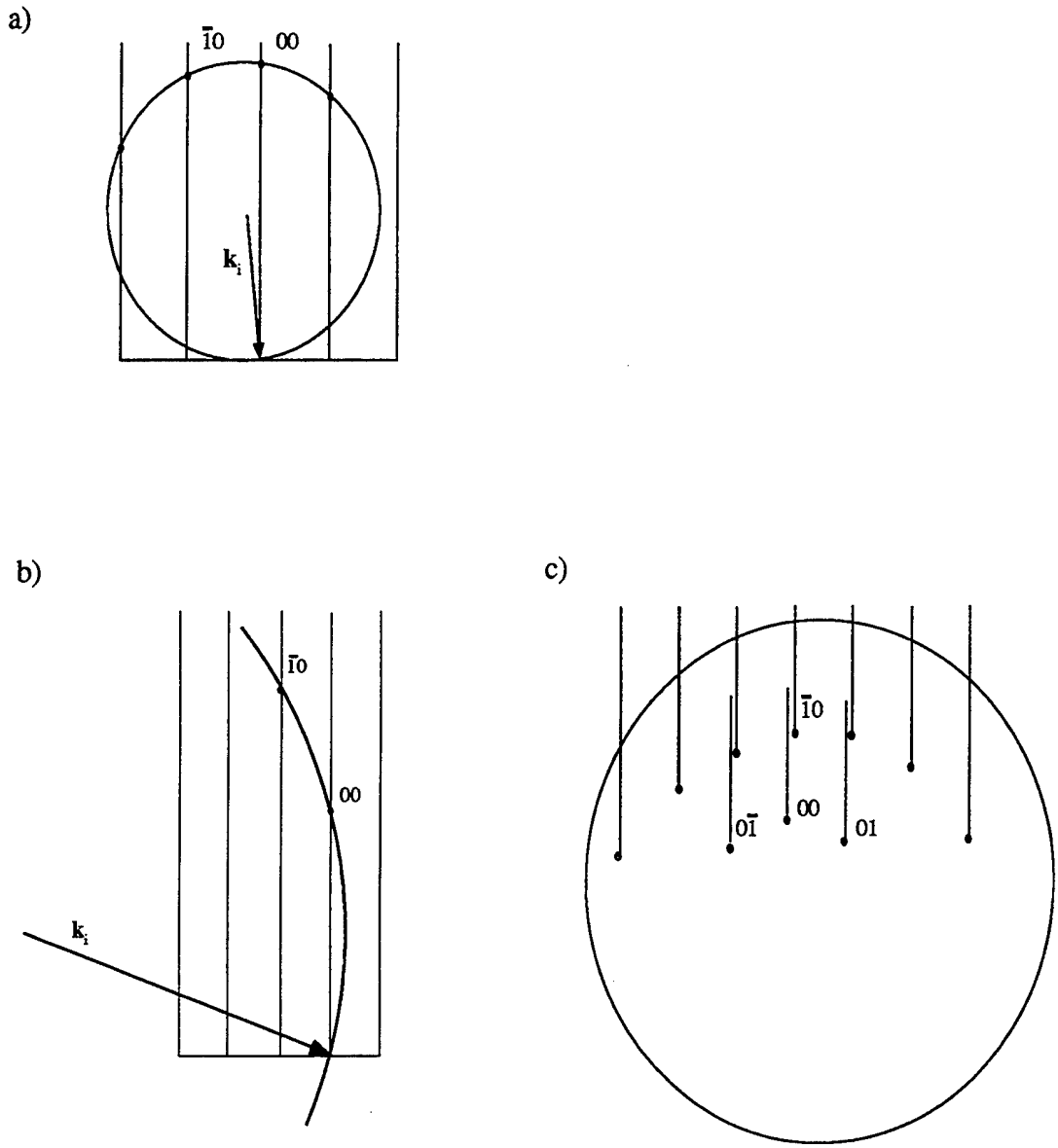

Figure 1.2 a) The Ewald sphere construction is shown for LEED. The incident wavevector is nearly parallel to the reciprocal lattice rods. b) The Ewald construction for RHEED is shown. The angle between the incident beam and surface, exaggerated in the figure, is small and the incident wavevector is nearly perpendicular to the reciprocal rods. c) The Ewald sphere from part (b) is viewed from the direction of the screen. This view shows that the projection of the diffracted beams on the phosphor screen is the familiar arcs of spots observed using RHEED.

rod at a maximum and minimum respectively. Surfaces with a larger number of exposed levels will have rods that more closely resemble bulk reciprocal lattices.

Stepped surfaces possess two reciprocal lattices, one from the periodicity of the atoms on the terraces and a second from the periodic arrangement of steps. This is depicted in Figure 1.3. Neglecting the finite transfer width of the observing instrument, the reciprocal rods from the terraces are broader than the rods from a flat surface since the terrace consists of fewer scatterers. For instruments with a small transfer width observing relatively large terraces the rods due to the steps may actually be broader than the terrace rods. Diffraction spots from stepped surfaces will correspond to where both reciprocal lattices simultaneously intersect the Ewald sphere. This may cause the appearance of spot splitting at certain diffraction conditions. The splitting is usually observed as two separate peaks at the out-of-phase condition, but the observation of three peaks is possible depending on how the Ewald sphere intersects the rods. It can also

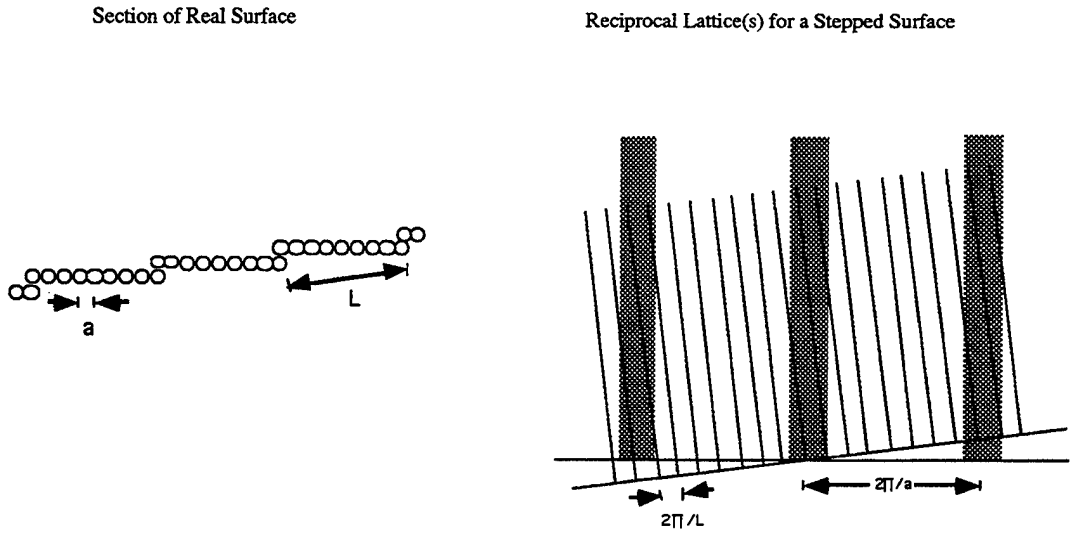

Figure 1.3 The right portion of the figure shows the reciprocal space lattice rods corresponding to the stepped surface depicted on the left.

occur that the spot is split into two spots which are observed only individually at separate diffraction conditions on either side of the integer order spot. While a surface of uniformly separated steps is possible, surfaces can also have a distribution of terrace sizes. This will lead to a broadening of the spots which in some cases can obscure the splitting.

Figure 1.4 shows the intersection of an Ewald sphere as drawn for RHEED with a single broadened terrace rod and two step rods for two incidence directions. Note that the glancing incidence angle used in RHEED causes the Ewald sphere to intersect the step rods at different heights. This causes the observed splitting when plotted as a function of the parallel component of the scattering vector not to equal the separation of the step rods as it would to good approximation in LEED. The figure also points out that spot splitting will be more pronounced when the beam is incident from the lower side of the staircase

Another interesting feature is the observation of satellite peaks in spot profiles on either side of the integral-order spots. These can be caused by a sharply peaked distribution of island separations. Usually these satellite peaks have much weaker intensities than the peaks of the integral-order spots so they are better observed with instruments that have a larger dynamic range than video-monitored RHEED such as SPA-LEED (spot profile analysis LEED). However, their explanation is instructive of some of the concepts that can be used in the analysis of RHEED spot profiles. Part (a) of Figure 1.5 shows a perfectly periodic structure of islands and the new rods introduced to the reciprocal lattice by the presence of this overlayer. The separation of the new rods is inversely proportional to the island separation. If the separation between islands were not constant, these rods and the diffraction spots corresponding to them would not exist. However, when islands are separated by a variable distance it is possible that the distribution function that describes their separations may be sharply peaked enough to allow satellite peaks to be seen. Part (b) of the figure shows a possible distribution

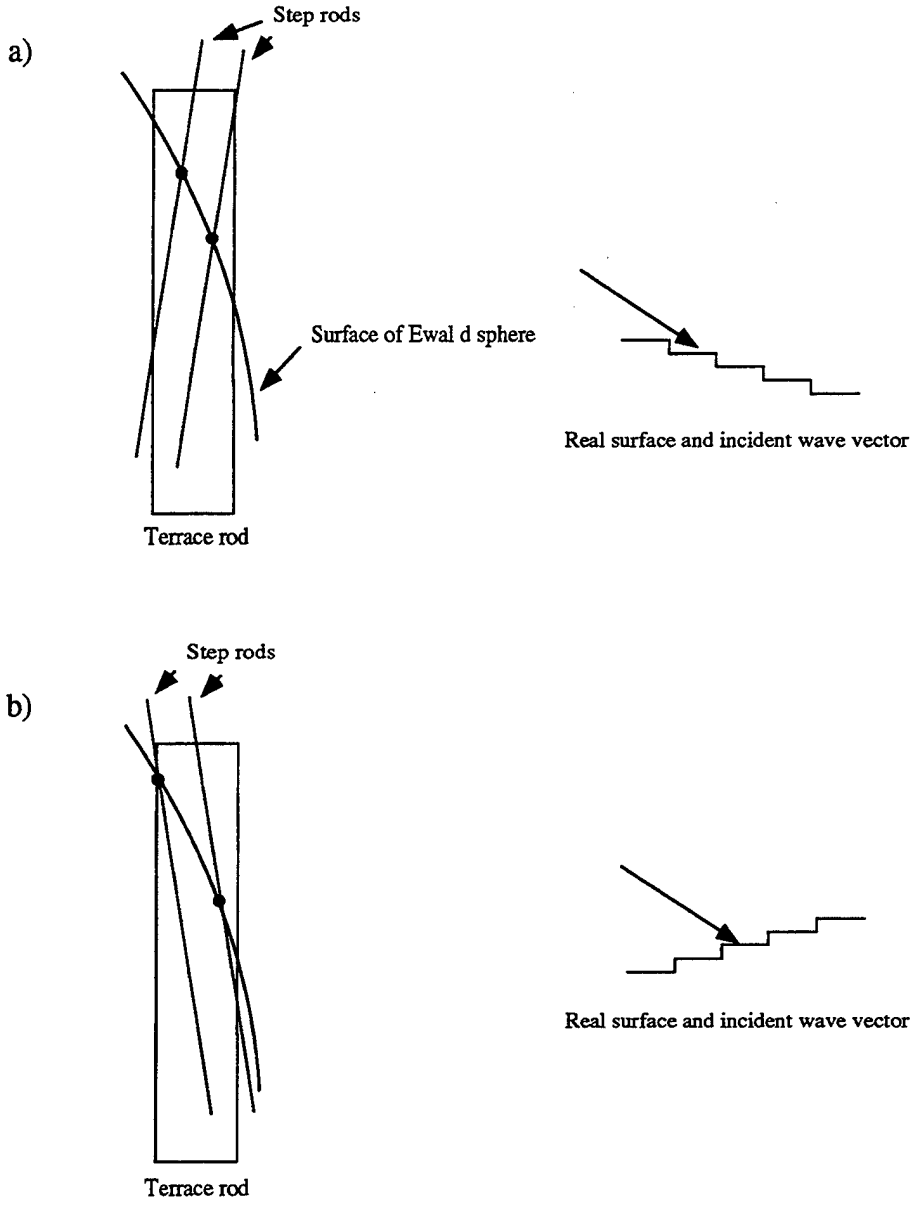

Figure 1.4 a) A single reciprocal lattice rod from the terraces is shown along with two rods from the steps. The Ewald sphere is drawn for the RHEED case where the incident wavevector is incident from the top of the steps. b) The same rods as in (a) are shown, but for the case where the incident wavevector comes from the bottom of the steps. In both cases the Ewald sphere intersects the step rods at different heights affecting the observed splitting, but the effect is more pronounced in (b) where incidence is from the bottom of the steps.

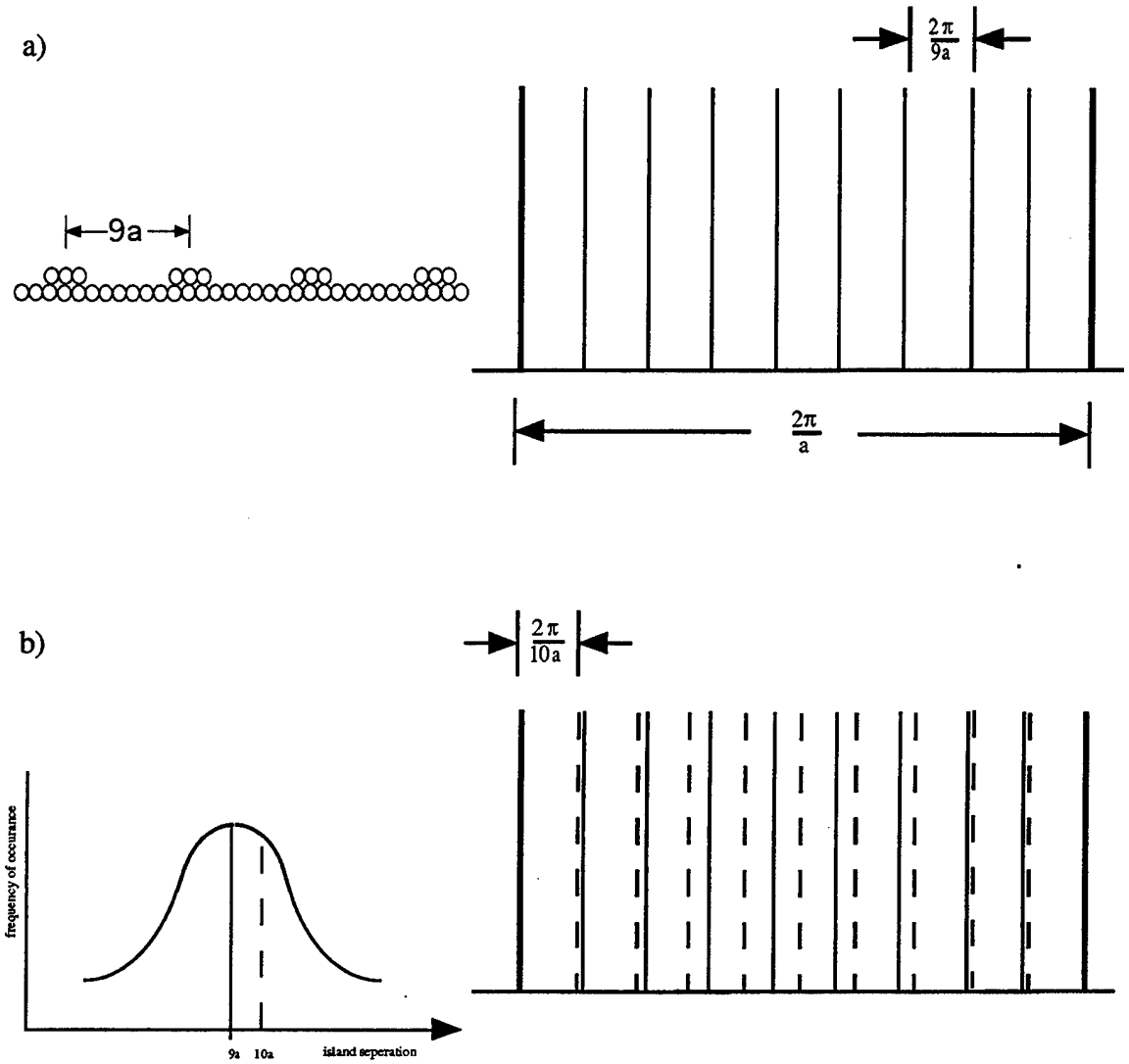

Figure 1.5 a) A surface covered by a periodic array of islands is shown and the corresponding reciprocal space rods. b) A distribution of island separations is assumed with a mean separation identical to part (a). The reciprocal space is approximated by the summation over all possible separations of the reciprocal rods that would exist if only that separation were present. Only the rods from two terms of this sum are shown to demonstrate that weak satellites may occur at the location of the rods corresponding to the mean separation and that these satellites are strongest near the integral order rods where the many terms from the sum will almost add coherently.

function of island separations with an average separation the same as that used in part (a). While not entirely correct, the presence of satellites can be understood qualitatively by considering the reciprocal lattice for a surface covered by such a distribution of islands as the combination of the reciprocal lattices of each possible separation. Figure 1.5 shows the combination of only two terms to demonstrate that the distribution washes out the additional rods seen in the first part of the figure with rods further from integral-order spots being affected the most. For real, two dimensional surfaces covered by islands with a sharply peaked distribution of separations the reciprocal lattice may consist of weak concentric rings around the integral order rods.

Spot profiles are often analyzed [20, 21] by breaking them down into two parts, a sharp central peak and a broader, weaker peak. The observed spot is then the summation of the intensities from these two contributions, each of which is often assumed to posses a Gausssian shape. For high quality crystals the width of the central peak is limited by the instrument response, and the width of the broader peak is taken as inversely proportional to the average separation of surface features such as steps or islands. This can be considered a special case of the situation described in the previous paragraph where the distribution is so broad that no splitting is resolvable. At the in-phase condition where the pattern is insensitive to interference between layers the broader peak should vanish, and conversely the central spike should not be present at the exact out-of-phase condition. During layer-by-layer film growth, the inverse of the halfwidth of the broader portion at the out-of-phase condition represents the average island size for large islands, or the average island separation for small islands.

In analysis of film growth it is often easier to monitor only the peak intensity of a diffraction spot. This is justified in cases where the normalized spot profiles do not change. In other cases, the changing spot profile indicates that the broader of the two components described above is not constant, and since the sharp central peak almost

always changes with coverage monitoring only the peak intensity would not allow the contributions from the individual components to be sorted out. In the current study, no changes in the normalized spot profiles were observed during deposition, and much analysis was done using the peak intensity of the specular beam which, other than a constant background, was assumed to be the intensity of the central peak.

In RHEED it is not uncommon to observe a diffraction pattern that contains streaks instead of spots. While there have been various other explanations offered for this phenomenon in the past, the streaking is caused by the grazing angle at which the Ewald sphere intersects the reciprocal lattice rods. If the reciprocal rods are broad enough, streaking will result. In the current study, streaking was observed when silver was deposited onto the silicon samples.

The grazing angle at which the Ewald sphere intersects the reciprocal lattice rods is also responsible for the high resolution in one direction obtained by RHEED. Because of this, it is usually not possible to see spot splitting from stepped surface when the beam is incident parallel to the step edges.

Due to complications such as multiple scattering, accurate calculations of what the real RHEED spot intensities would be for a given surface are not currently feasible. However, using the kinematic approximation which neglects multiple scattering and treats all atoms of the same type as identical scatterers, information about the spot shapes that correspond to a given surface may be obtained. In this approximation the intensity, I, is given by

$$I(\mathbf{S}) = \left| \sum_{\mathbf{r}} f(\mathbf{r})\, e^{-i\mathbf{S}\cdot\mathbf{r}} \right|^2 \qquad (1.3)$$

where **S** is the momentum transfer (the difference between outgoing and incoming wavevectors), **r** is the position vector for an atomic scatterer, and $f(\mathbf{r})$ is the scattering factor. More correctly, the scattering factor should be a function of energy and angle, but

for the nearly monoenergetic beams used in diffraction the energy dependence is usually neglected, and complications from the angular dependence are usually not worth considering in simulations designed just to see if a particular surface could be responsible for an observed diffraction pattern. The kinematic approximation is discussed on more detail in appendix A and was used for the simulations described in Appendix B.

2. EXPERIMENTAL SET UP

These experiments were performed in a turbo pumped vacuum chamber with a base pressure of 4×10^{-11} Torr. The RHEED apparatus consisted of a 5 keV electron gun and a phosphor screen placed on opposite sides of the sample. A rotary feedthrough allowed the sample to be rotated about one axis. For most of the experiments the electron gun was mounted in a fixed position, and although later an off-axis port aligner allowed the electron gun limited movement, in practice the incident angle was adjusted by rotation of the sample. Images of the diffraction pattern appearing on the phosphor screen could be viewed directly or captured by a video camera and digitized for later analysis.

The silver deposition source consisted of a graphite crucible filled with silver powder which was heated by passing a current through ceramic insulated, tungsten wires placed within slots machined into the back of the crucible. The source was equipped with a shutter, and the flux rate could be varied by choosing different heating currents. The source was capable of producing flux rates with monolayer (ML) completion times that ranged from 30 seconds to 90 minutes. These flux rates were calibrated using the completion times of low temperature RHEED intensity oscillation and independently by temporarily replacing the sample holder with a quartz crystal monitor. Unless otherwise noted the films discussed used a deposition flux rate of 1 ML/2 min.

For experiments that required quickly changing the deposition flux rate the source's shutter was equipped with a small hole. Two flux rates were then available for

any given crucible temperature, one with the shutter adjusted so that the small hole was over the crucible and the other with the shutter completely uncovering the crucible. These two flux rates differed by roughly a factor of six. Figure 2.1 shows the shutter design and data from the quartz crystal monitor for depositions using both shutter positions.

The silicon samples were obtained from 10 mil thick, phosphorus doped wafers purchased from Virginia Semiconductor. Rectangular samples approximately 4 x 12 mm were produced by breaking the wafers along lines that had been scribed with a diamond scribe. All samples had resistivities between 0.03 and 0.08 Ohm-cm. The samples were mounted onto a sample holder between tantalum clips. In addition to attaching to the rotary feedthrough, the sample holder was connected to an external dewar by a copper braid to allow for cooling using liquid nitrogen. The sample could also be heated by passing a current through it; this in conjunction with the liquid nitrogen cooling allowed temperatures anywhere between 170 K and the sample's melting point to be obtained. At various times thermocouples were attached to the tantalum clips that held the samples to determine temperatures, and above 600^0C the sample's temperature could be monitored through a viewport with an infrared pyrometer.

The samples had originally been coated with an oxide layer by their supplier. This layer was easily removed by heating. However, the samples were outgassed for approximately twelve hours at temperatures below those necessary to remove the oxide first to prevent surface roughening from occurring. It has been reported [22], in agreement with the author's experience, that at pressures much above 10^{-9} Torr Si(111) surfaces will roughen at elevated temperatures. The samples were further repeatedly heated to approximately 1250°C so that many layers of silicon sublimated from the sample. This method was employed since the chamber used in this experiment was not equipped with an Auger system, the most common means to detect surface

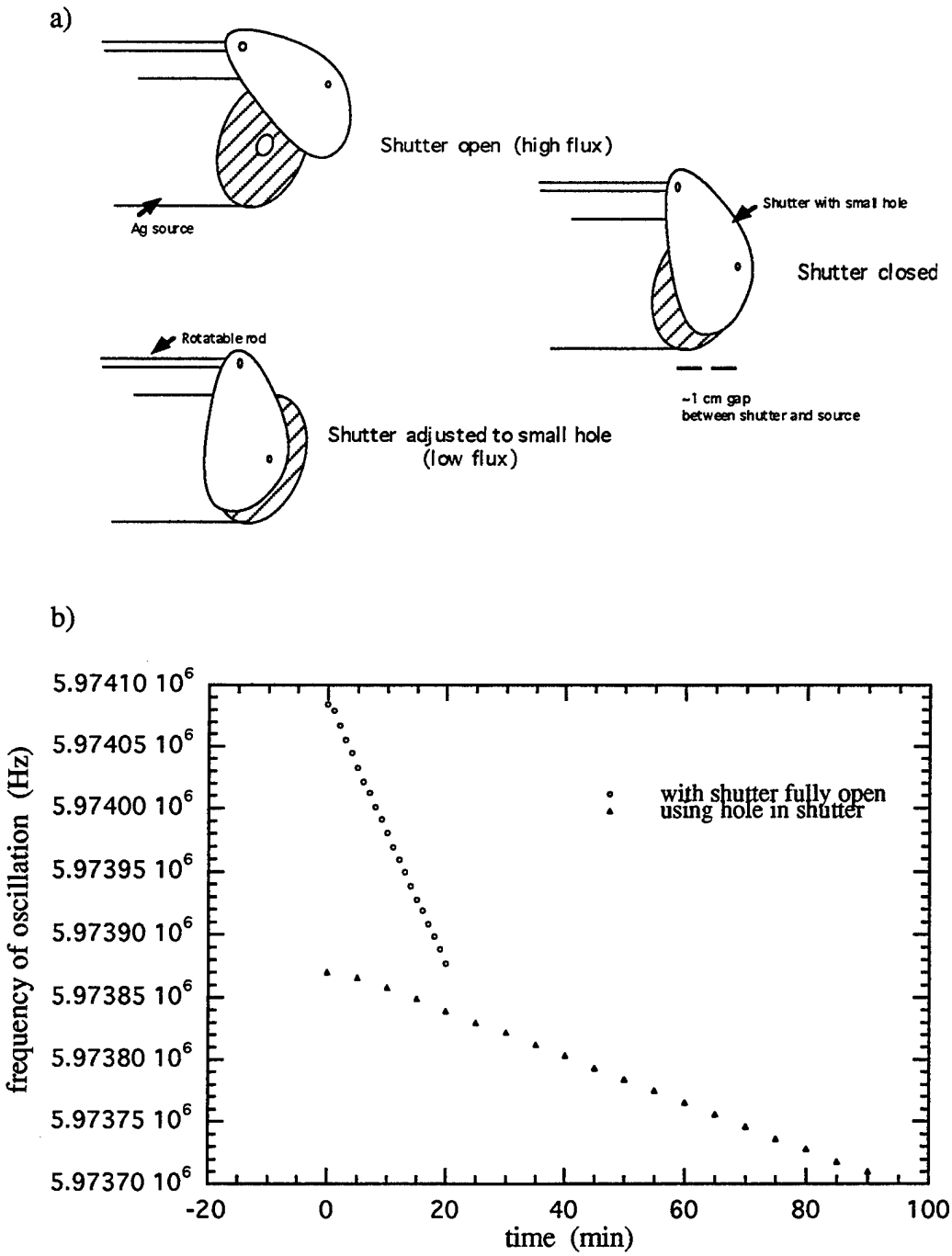

Figure 2.1 a) The design of the shutter used in the multiple flux experiments is shown. b) The oscillation frequency of the quartz crystal monitor during two depositions identical except for the use of the small hole in one and not the other. The crystal's frequency shift is proportional to the mass of the deposited film.

contamination, and Auger electron spectroscopy used in previous studies of the Si(111) surface has shown such surfaces to be free of detectable levels of contaminants after heating for 5 min. at temperatures as low as 1050°C [23].

While each sample was initially, and occasionally at other times, cleaned by sublimation to expose a new surface, a less rigorous procedure was used before each experiment. The samples were heated to above 1000°C for between 15 seconds and two minutes then the temperature was reduced and held at approximately 750°C for between 2 and 5 minutes. The exact cleaning temperatures and the time it was held at each temperature varied over the course of these experiments, but were kept identical for any given set of runs.

The angle of incidence could be determined using pictures which showed both the specularly reflected and the so-called through beam, that portion of the beam which passes around the thin sample and continues toward the screen undeflected. Miscut angles of the vicinal samples could be determined using the positions of the specular, through beam, and the location of the shadow edge beyond which there was no diffuse scattering. Figure 2.2 shows how the incidence angle was determined from information available on the phosphor screen, and Figure 2.3 shows the procedure for determination of sample miscut angles from the same information. In some cases it was desirable to observe diffraction patterns from two different beam incidence directions. The limitations of chamber's motion feedthrough and sample holders required that a new rectangular sample be cut and installed for each incidence direction desired. To observe spot splitting and obtain information about step spacing the beam was incident perpendicular to the step edges from either the $[2\bar{1}\bar{1}]$ or $[\bar{2}11]$ direction. The $[0\bar{1}1]$ direction was used to observe the dimensions of silver crystallites parallel to the step edges and in an attempt to observe small angle intensity oscillations on the vicinal samples.

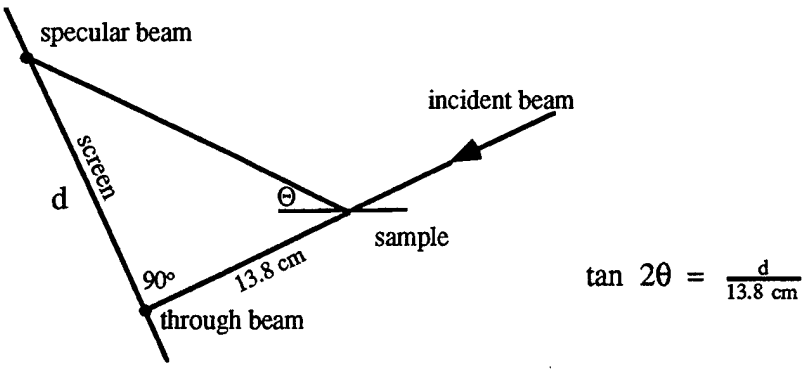

Figure 2.2 Using the measured distance between the specular and through beams, d, and the sample to screen distance of 13.8 cm the incidence angle could be determined.

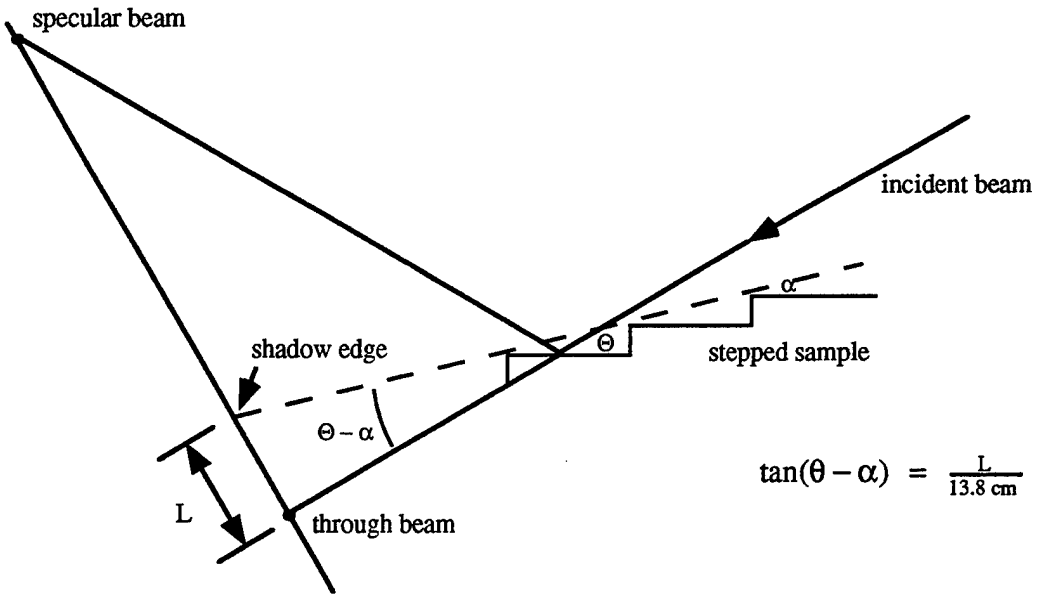

Figure 2.3 The position of the shadow edge, specular, and through beams allowed the miscut angles of the stepped samples to be determined using beam incidence perpendicular to the step edges. The diagram above depicts incidence from the uphill direction. For incidence from the downhill direction the left-hand side of the above equation becomes tan(Θ+α)

A video camera was used for real-time image acquisition. Since a blue phosphor screen was used, the camera was equipped with a tube most sensitive in this region of the spectrum to allow images of even fairly dim spots to be recorded. The video signal was digitized by an 8-bit A/D board and images saved onto a hard disk. The through beam was masked by tape so as not to saturate the camera when images of the diffraction pattern were taken. The hard disk could hold only a few months of data so older data was periodically transferred to tape or floppy. Software developed within the group allowed for viewing of the images and simple data analysis. Often only that part of the picture which showed a small part of the pattern or a single spot was saved due to either disk space considerations or a desire to take pictures in quick sequence. Full 480 x 512 pixel images required approximately 2.5 seconds to save to disk while 60 x 60 pixel frames showing only a single spot could be saved at the rate of three per second.

3. SILVER GROWTH ON FLAT SILICON (111) 7 x 7 SURFACES

3.1 Introduction

Silver deposition on the (111) surface of silicon has been performed by many researchers [1,8,24-30]. Normally these silver films grow in a 3D structure if deposited above room temperature while at lower temperatures quasi layer by layer growth can be achieved. Some researchers have succeeded in inducing layer by layer growth to occur in other systems, such as Ag on Ag, by using surfactants [31-33], a low temperature predeposition [33], or periodic sputtering [33]. This section describes experiments which include one in which RHEED oscillations observed during the deposition of Ag onto the 7 x 7 Si(111) surface at 220K were slightly enhanced by an initial high burst in the flux of arriving atoms. Like at least some of the methods that have been used to induce layer by layer growth in other systems, this enhancement of the low-temperature oscillations is caused by an increase in the island nucleation density. The enhancement of low-temperature RHEED oscillations during silver deposition onto the (111) surface of silicon by an initial high burst of flux along with the methods of inducing layer by layer growth at higher temperatures mentioned above would seem to imply that the temperature dependence of the island nucleation density is at least in part responsible for the oscillations observed at low temperatures. This does not, however, rule out the operation of a possible nonthermal growth mechanism, as discussed in chapter 1.

3.2 Temperature Dependent Growth

When silver was deposited on the flat silicon samples the simplest, and most common, observation was monitoring the peak intensity of the specular beam as a function of time. For depositions much above room temperature the peak intensity of the specular beam decayed monotonically with time, reaching a nearly constant value after approximately one monolayer had been deposited. For depositions at lower temperatures damped oscillations in the intensity of the specular spot were observed with the number and quality of the oscillations increasing with decreasing temperature. The oscillations could also be improved by decreasing the angle of incidence of the electron beam. Unfortunately, during the time that most of these experiments were performed, light coming from the filament of the electron gun put a practical lower limit on the usable incidence angle of about one degree limiting the quality of the oscillations that could be observed.

The improvement of the oscillations with decreasing angle did not coincide with nearing an out-of-phase condition, and the author does not know the explanation for this behavior. However, some authors [34,35] have modeled diffraction from surfaces during growth by using a one dimensional scattering potential for the surface which increases in magnitude with the coverage of the growing film. Reflection coefficients are then calculated for various coverages by solving the Schrödinger equation. The intensity is then calculated in the kinematic approximation using these reflection coefficients as the atomic form factors for atoms of the appropriate layers. Horio and Ichimiya [35] have used such a potential to show that the magnitude of the oscillations calculated using their model increases in agreement with experiment as the angle of incidence is decreased. They have also compared their one dimensional model potential to a more realistic 3D model and find qualitative agreement in the calculated oscillations. These one-

dimensional models also reproduce a frequency doubling sometimes observed experimentally which results in two maxima per period. One of the two maxima is calculated to be much weaker than the other. Close examination of Figure 1.1 will show a small maximum shortly after the first minimum. This is in qualitative agreement with the calculations from the one-dimensional models if it is assumed that the secondary, smaller maxima are too weak to be detected in subsequent periods.

Figure 3.1 shows the evolution over time of the intensity of the specular beam for depositions at temperatures ranging from 226 to 310K using an incidence angle of 1.5°. This figure displays three properties which were consistently observed at this angle. First, the quality of the oscillations increases for lower temperature runs (the maxima rise higher from the minima, and although weak, additional maxima can be seen). Second, the maximum intensity following the first minimum occurs later for runs performed at lower temperatures. The third observation is that the final, so called, saturation intensity is a function of temperature with lower temperature runs having higher saturation intensities. The angle used for the runs shown in Figure 3.1 is very near an out-of-phase condition where interference from the reflections of different levels should have the largest effect. The observed dependence of the saturation intensity on temperature implies that the films grown at lower temperatures are smoother with fewer exposed levels. Figure 3.2 shows a series of runs performed at 0.8°, an in-phase condition. At this angle the intensity is insensitive to the interference between levels and the saturation intensity is almost independent of temperature.

Figure 3.1 shows that runs with better oscillations have longer periods, at least for the first oscillation. This has been seen before for Ag on Ag(100) [36]. In the perhaps oversimplified picture where the oscillation maximum corresponds to monolayer completion, as it would for perfect layer by layer growth, this would imply that when the first layer fills there are more atoms already in the second layer for those runs that show

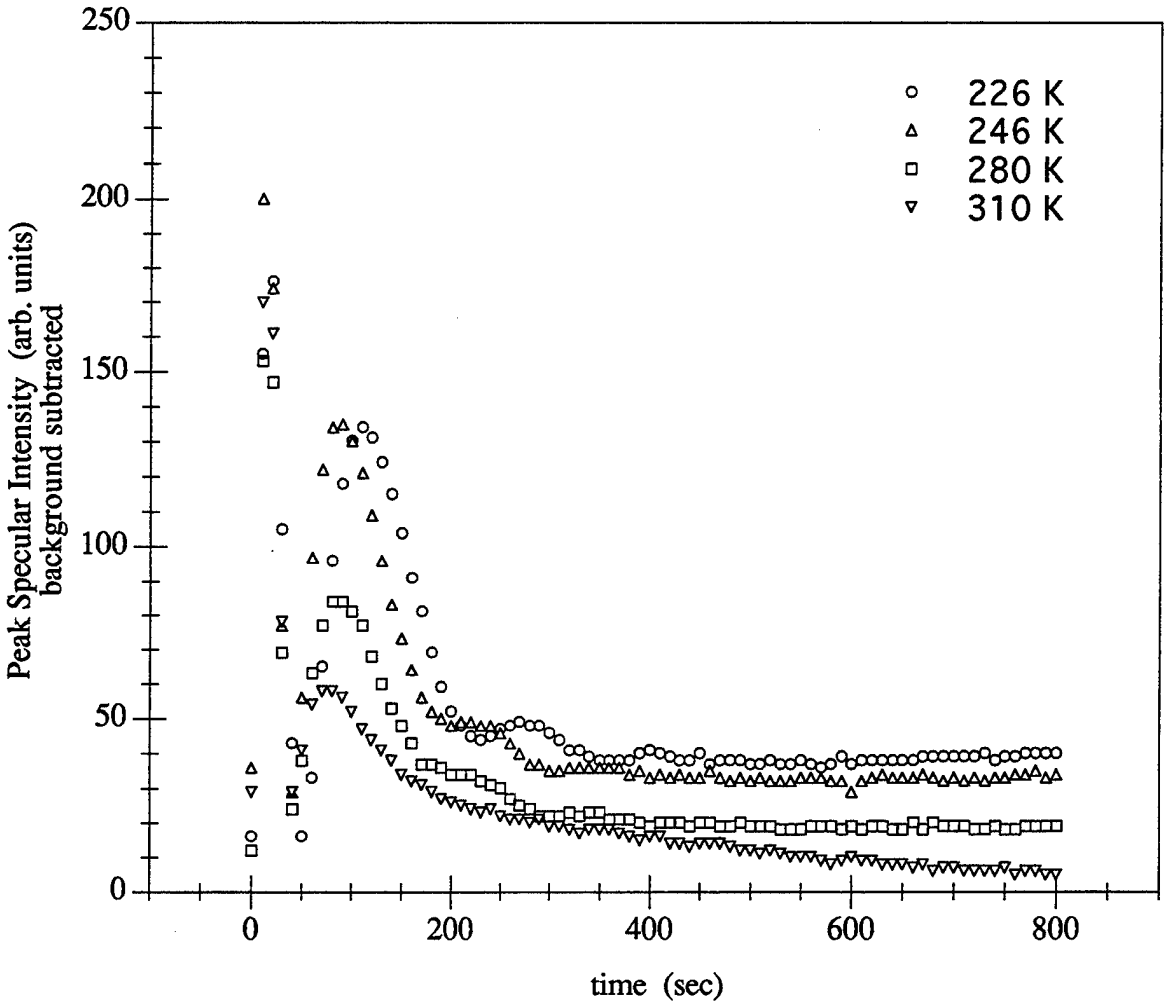

Figure 3.1 Oscillations of the specular intensity during the growth of silver films on silicon (111) are shown for four temperatures. The incidence angle was 1.5°, very near an out-of-phase condition.

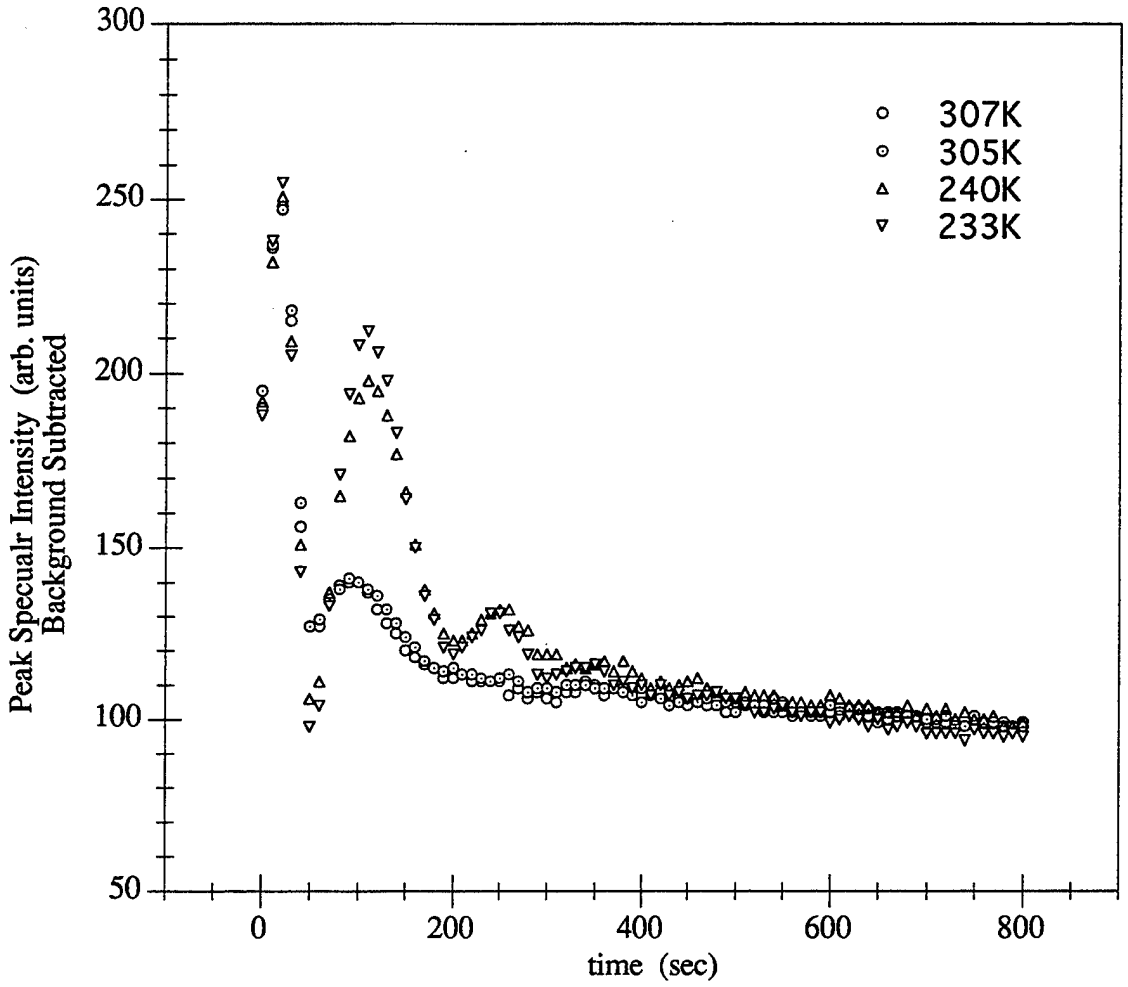

Figure 3.2 Oscillations of the specular intensity during the growth of silver films on silicon (111) are shown for four temperatures. The incidence angle was 0.8°, at an in-phase condition

better oscillations. This implies that good layer by layer growth of the initial layer results in rougher growth in subsequent layers. This, however, is not necessarily the case since for imperfect layer by layer growth the assumption that the maximum occurs at layer completion may be incorrect. Where the maximum occurs is a difficult question to answer because of multiple scattering, sections of lower layers being shadowed from the incident beam, and the possibility of a different scattering factor at the step edges.

The explanation that RHEED intensity oscillations are caused by interference from the reflections from the exposed atoms on different levels does not explain how they can be observed at an in-phase condition as shown in Figure 3.2. One somewhat speculative explanation for this is that the intensity of the diffraction spots depends on the step edge density. Simulations done by Clarke and Vvedensky [37] have shown that the evolution of the step edge density corresponds well to the RHEED intensity oscillations observed during the growth of III-V compounds. Such a dependence could come about from a difference in scattering factors between the atoms at steps and those atoms not at island edges. For perfect layer-by-layer growth the step edge density periodically changes from zero at layer completion to a maximum at some point before island coalescence begins to reduce the number of atoms at edge positions. If the specular intensity depended both on the interference between levels and the step edge density it would be possible to explain the occasionally observed double periodicity of RHEED oscillations previously discussed.

3.3 Flux Burst Enhanced Intensity Oscillations

Several runs were performed that tried to enhance the low temperature intensity oscillations by altering the flux rate during deposition. Figure 3.3 shows the comparison of two low temperature runs, one of which has an initial burst in the flux rate of arriving

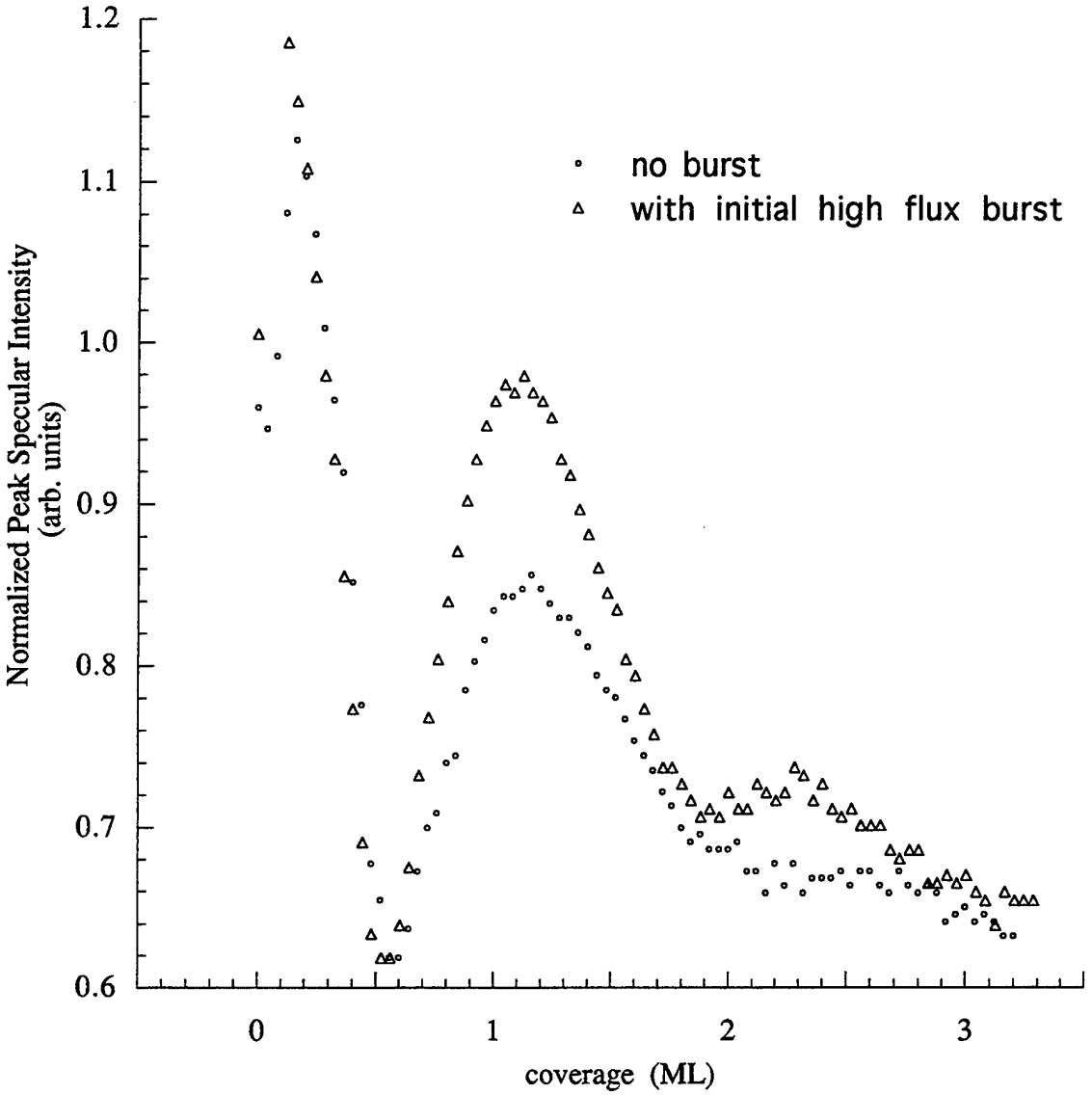

Figure 3.3 The normalized peak intensity of the specular beam is displayed for two depositions. One used an initial high burst in the deposition flux rate, and the other did not. Both runs used a temperature of 220K.

atoms. The run with the flux burst shows a somewhat enhanced oscillation. An attempt was made to increase the number of oscillations by periodically applying a burst of flux. In separate runs, flux bursts were applied at, before, and after the expected monolayer completion time. However, none of these additional bursts of flux were observed to affect the oscillations. Flux bursts of various lengths were tried with most experiments using a burst of flux that deposited one tenth of a monolayer.

An increased island density leads to smoother films as atoms arriving on top of the smaller existing islands are more likely to diffuse to the edge and therefore have an increased chance of descending before they nucleate yet another level. Dendritic shaped islands also favor smooth growth for the same reason and have the added possibility of increasing interlayer transport in the presence of a step edge barrier by reducing the barrier at kinks. Either an increase in the island density or a temperature dependent island shape could explain the improving quality of the observed oscillations with lower temperature. However, it seems unlikely that lowering the temperature and the use of a flux burst would both alter the shape of the islands. This would seem to point to an increased island density as being responsible for the improved oscillations at lower temperatures.

A possible explanation for why additional flux bursts beyond the first were not observed to affect the oscillations is that the increased mobility of the Ag adatoms on silver allowed islands to nucleate so far apart that the expected doubling of the island density from the flux burst still produced islands large enough to prevent atoms arriving on top of them from descending before nucleating a new level. Vrijmoeth et al. [32] have observed an average island separation of 3500 Å for room temperature growth of silver on silver using a similar flux rate. Also, such a small island density would lead to an increased importance of any defect induced nucleation.

3.4 Lattice Constant Observations and Strain

The silicon substrate acts as a template for the growth of silver, and since the conventional bulk unit cells of silicon and silver have lattice constants of 5.4 Å and 4.1Å respectively there must exist some mechanism to relieve the strain caused by the mismatch in lattice constants. One possibility for such a mechanism is the straining of the silver lattice constant to match that of silicon for the first layer, followed by a subsequent reduction in strain with each additional layer until the film achieves the bulk lattice constant for silver. Another possibility is that silver films form with the usual silver lattice constant, but form in crystallites of limited dimensions so that each crystallite can be nearly optimally oriented on the silicon with the lattice mismatch being compensated for at the domain boundaries. While the first possibility might offer an explanation for the damping out of RHEED oscillations over a few monolayers, the latter is more consistent with the observed data.

The diffraction data from several films was examined to see if a detectable change in the lattice constant could be seen as the films grew. The lattice constant is inversely proportional to the streak separation so this separation was monitored as a function of coverage. In principle this is a simple procedure consisting of measuring the separation between the silver streaks that appear in the diffraction pattern and comparing the values for different coverages. However, complications arise because the intensity of the streaks is weak at low coverages and this makes the uncertainty in the measurement of their location largest for the data that is most crucial. An additional experimental difficulty encountered was that after cleaning the sample the electron beam drifted detectably even after an hour. However, no detectable change in the lattice constant was observed for any of the films analyzed implying that a changing lattice constant was not responsible for the necessary strain relief. The uncertainty in the measurement of lattice constants is

estimated at 3% for films consisting of at least one monolayer, and drops to 1% for films exceeding five monolayers. Films grown both at room temperature and below were examined in this manner. Lattice constants were determined out to 25 monolayers. Figure 3.4 shows the streak separation of one film as a function of coverage and a profile parallel to the shadow edge showing the specular spot and two silver streaks.

Gotoh and Ino [24] have reported that silver grows preferentially with the orientation $[01\bar{1}]_{Ag}//[01\bar{1}]_{Si}$ on $(111)_{Ag}//(111)_{Si}$. Indexing the diffraction patterns observed in this study showed silver to grow only in this orientation. None of the diffraction spots corresponding to the second orientation observed by Gotoh and Ino were ever seen.

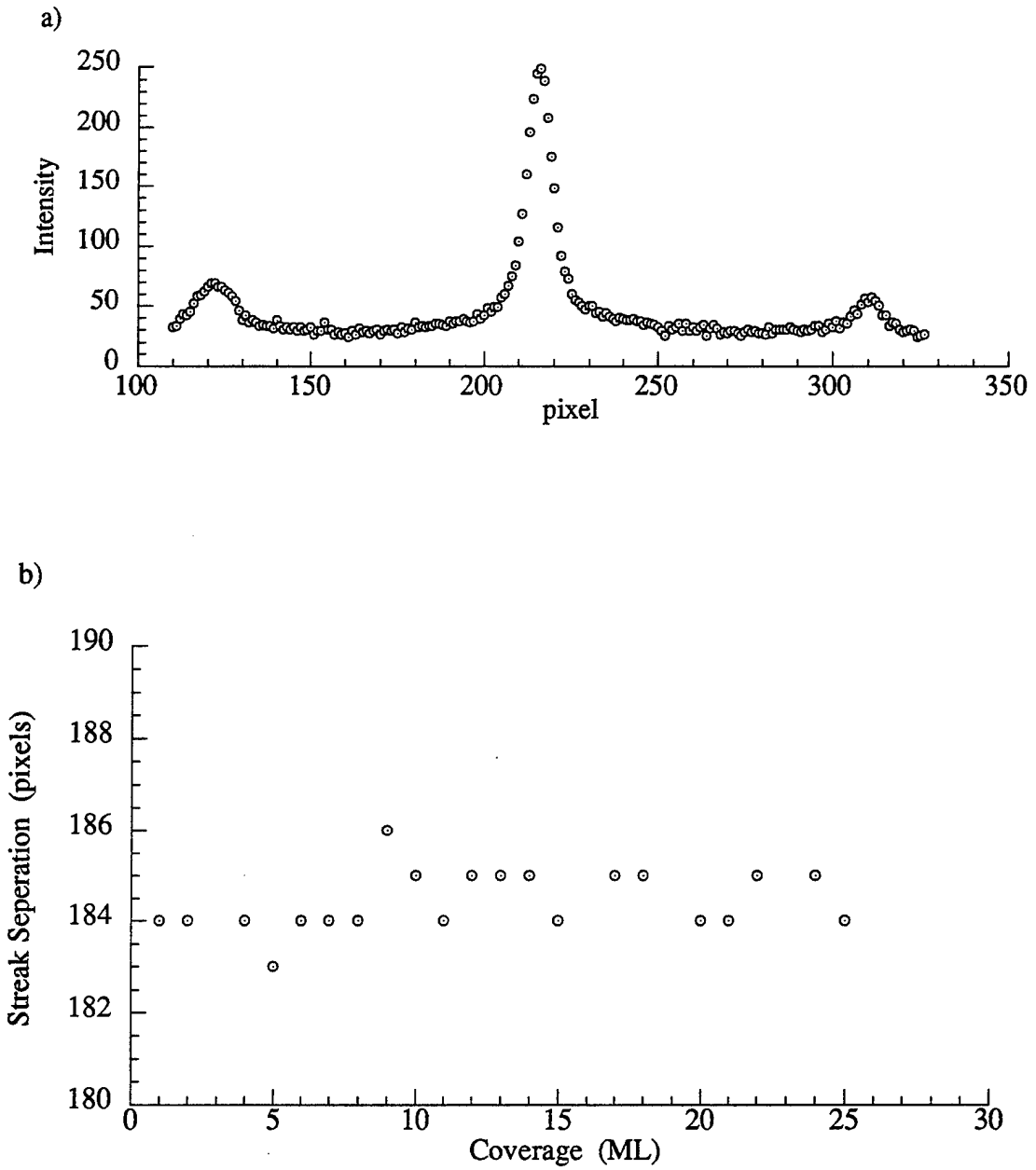

Figure 3.4 a) A profile parallel to the shadow edge shows the specular and two silver streaks at 5 ML coverage. b) The streak separation of a silver film deposited at room temperature is plotted as a function of coverage.

4. VICINAL SILICON SURFACES

Silicon samples miscut from the (111) plane towards the $[2\bar{1}\bar{1}]$ direction by 1.2°, 2.5°, and 4.5° were studied. Initially, the integral-order spots all showed splittings characteristic of surfaces containing uniform steps. Following the same procedure for cleaning of the samples as used on the flat surfaces, no changes in the width of the spot splittings were observed as the sample was cooled back down to temperatures where the 7 x 7 reconstruction could form indicating that the size of the terraces remained constant during the phase transition. However, since step bunching had previously been observed during the 1 x 1 to 7 x 7 transition for other miscut directions of the (111) surface by others [11-13], attempts were made to imitate their cleaning procedures which cooled the sample much more slowly through temperatures in the region of the phase transition. After using this special cleaning procedure the spot splitting vanished, and sharp specular profiles were observed. It seems likely that the splitting vanished as a result of formation of large terraces of the (111) plane interspersed with bunches of steps. It was possible to reobtain the splitting by repeated flashing to temperatures at which silicon sublimated. Later, the disappearance of the splitting was monitored during the transition, and the width of the splitting remained constant until it disappeared. This would indicate that a few large terraces, probably the ones that the 7 x 7 first nucleates on, grow while the others remain a fixed size until being incorporated into one of the few growing terraces.

While it has been reported before [18] that Si(111) miscut in this direction forms triple steps, no evidence for this was ever observed during the experiments described here. While on many occasions the observed splitting would correspond to terraces that

required step heights greater than one atomic plane to match the known miscut angle, the author interpreted these occurrences as being explained by the presence of step bunching on other parts of the surface. This seemed reasonable as after the steps had been deliberately bunched it took much effort to return the surface to its original state. The previous studies which reported the formation of triple steps where performed by LEED and used silicon with miscut angles of at least 6°. It should be noted that their surfaces also showed splitting with corresponding terrace sizes that were not consistent with both the step height and miscut angle, suggesting compensating regions of step bunching on other parts of their surfaces. It is possible that the samples used for the research of this thesis had step densities too low to observe the behavior previously reported. Another possibility is that the observation by Becker et al. [38], that the terraces they observed always contained an integer number of complete 7 x 7 unit cells with no left-over atoms, is a strict requirement for all terraces containing the 7 x 7. This could make the step configuration a function of miscut angle.

No splitting was ever observed in the fractional-order spots, and except as noted below, the integral-order spots all showed splitting at the same phase conditions. This observation indicates that the step edges are separated by integral multiples of the primitive lattice vectors, but non-integral multiples of the lattice vectors for the 7 x 7 reconstruction. This is in agreement with the report of Becker et al. [38], who, using scanning tunneling microscopy, observed that the 7 x 7 cells of adjacent terraces were offset from each other by about 2/7th's of a 7 x 7 unit mesh. Their observations were made on surfaces miscut towards the $<11\bar{2}>$. Such a phase shift in the positioning of unit cells theoretically allows splitting to be seen since cells seven terraces apart will occupy identical positions. However, the finite transfer width of the instrument will cause the pattern to be insensitive to such long range correlations. After some samples had been

treated to produce step bunching the integral order spots from these surfaces no longer changed phase in unison. The origin of this behavior is unknown.

Figure 4.1 shows the evolution of the specular profile during the step bunching transition as the sample is slowly cooled back down and the 7 x 7 forms. The cooling rate was approximately 6 C°/min. The splitting is replaced by a single spot after the transition. During the transition the intensity of one of the peaks vanishes while within the uncertainty of the measurement, the position of both peaks remains unchanged. This would indicate that as the large terrace(s) grow they incorporate adjacent terraces without altering terraces much further away. Phaneuf and Williams [12], on the other hand, have observed a change in the width of the splitting during step bunching on Si(111) miscut towards the $[\bar{2}11]$. This change in splitting that they observed could be explained by a shrinking of all terraces except for the few growing ones.

Figure 4.2 shows a profile of the specular beam plotted as a function of the parallel component of the scattering vector (that component of the momentum transfer that is parallel to the surface) at an incidence angle of 4.9°. This angle is near an in-phase condition, and the incident beam is coming from the top of the steps. The single smaller peak observed is due to a rod belonging to the steps. Only one such peak is seen, and seen at an in-phase condition because the Ewald sphere intersects reciprocal space at different z-components for each peak as shown in Figure 1.4. If this surface were examined by LEED, where the Ewald sphere intersects the rods corresponding to the observed spots at almost right angles, a single unsplit spot would be seen at the in-phase condition and two symmetrical spots at the out-of-phase condition.

In LEED the observed splitting is approximately inversely proportional to the widths of the terraces, but the splitting observed in Figure 4.2, 0.045 $Å^{-1}$, is not a good approximation for the separation of the step rods because of the different z-components of reciprocal space at which they are intersected by the Ewald sphere. From the geometry

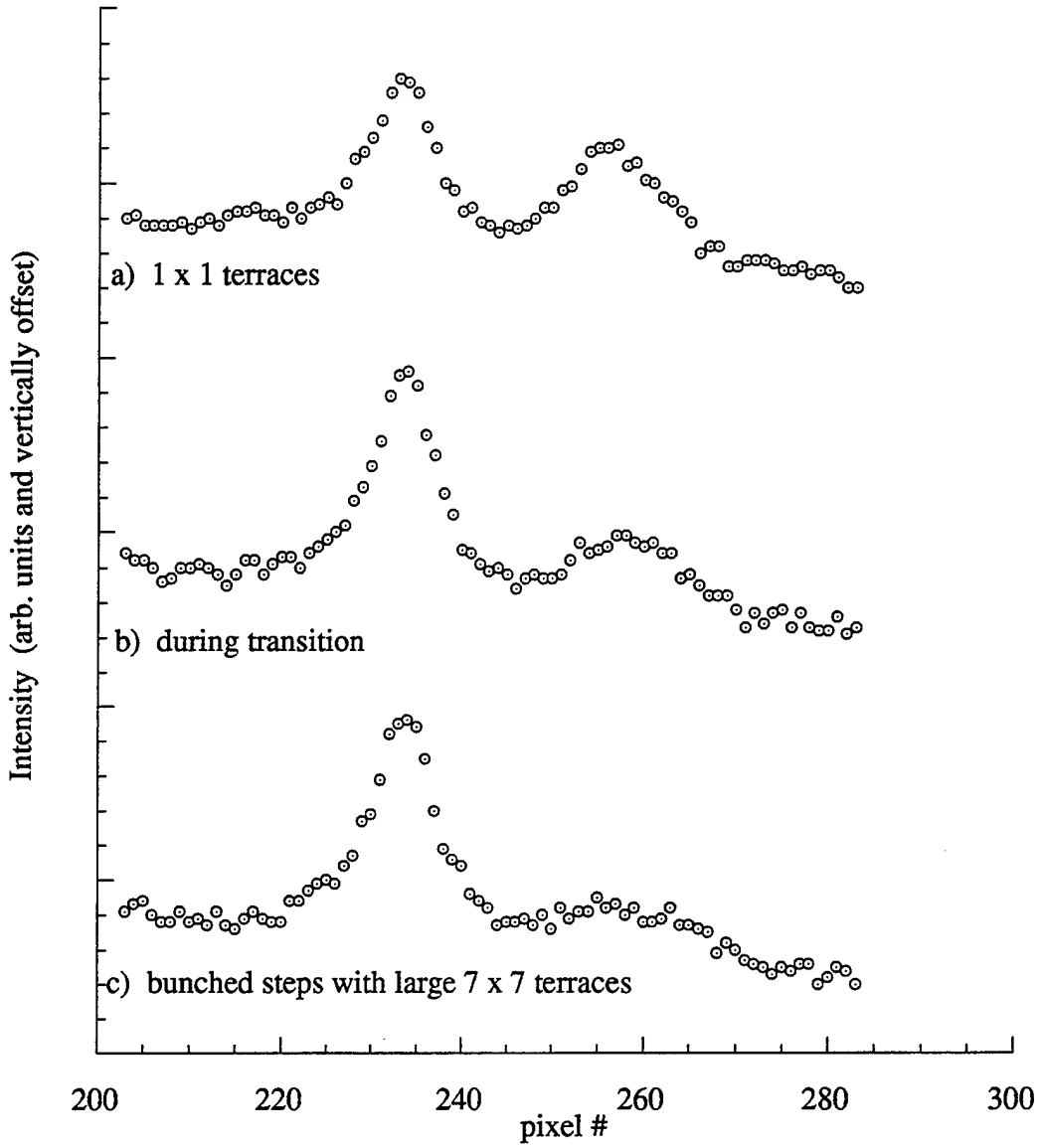

Figure 4.1 The evolution of the specular profile during the 1 x 1 to 7 x 7 transition is shown. The sample was cooled slowly enough to allow step bunching to occur. a) The split peak corresponding to a staircase structure of uniform terraces on the 1 x 1 surface. b) The profile during the step bunching transition. c) The unsplit peak after step bunching and the formation of large 7 x 7 terraces.

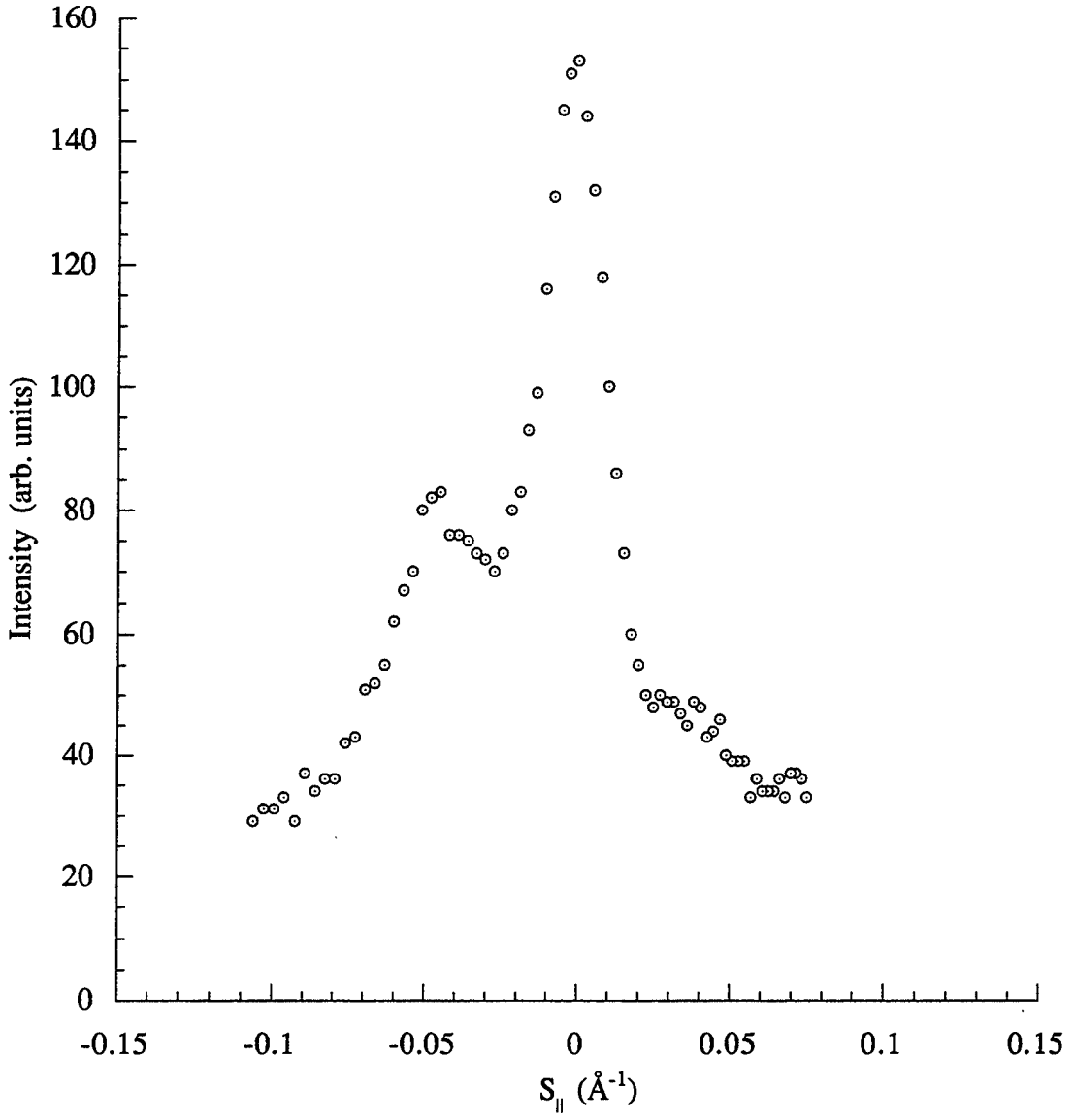

Figure 4.2 A profile of the specular beam from a clean vicinal silicon sample miscut by 2.5° is shown. The incidence angle is 4.9°, near an in-phase condition for the specular beam. The smaller side peak is due to a step rod and is seen at this angle because it has a different phase condition than the specular due to the different z-component of the scattering vector where the Ewald sphere intersects it.

depicted in Figure 1.4 the 0.045 $Å^{-1}$ observed splitting corresponds to a 0.068 $Å^{-1}$ separation of the step rods. This implies terrace widths of 92 Å. Considering just the known values of the miscut angle and the step height, terraces of 72 Å would be expected for a uniform surface. The observed terraces are probably larger than if the surface were covered by uniform terraces due to the presence of step bunching on portions of the surface.

At angles that produced a specular spot split into two nearly symmetrical peaks when the 1 x 1 structure was present (during heating) an asymmetry in the split spots would often develop as the sample cooled and the 7 x 7 reformed. This asymmetry looked like the asymmetry of the profile shown in Figure 4.2. Reheating to temperatures just below where the 1 x 1 was expected to form and then cooling the sample could change the magnitude or even reverse this asymmetry. It is possible that this could be explained by limited step bunching of the surface, but computer simulations were performed to search for other surface structures compatible with these observations. These simulations used the kinematic approximation, and with a single exception involved modeling the surface as stepped line of scatterers. This should yield the same results as modeling a three dimensional surface with straight, parallel step edges. Except for step bunching none of the model surfaces studied reproduced the asymmetry introduced as the 7 x 7 formed. Phaneuf and Williams [18] have also performed simulations similar to those of this work, and they too were unable to find a model surface that reproduced the features that they observed. It is possible that these models were too simple and that more complicated true three dimensional models with kinked steps, etc. might be able to reproduce all the experimentally observed features.

One model that offered a possible explanation for the changing asymmetry did not involve changes in the terrace widths, but instead changes in the scattering factors of the atoms making up the terraces. Uniformly stepped surfaces were modeled with each

terrace being identical in construction. The scatterers near the downward step edge were given a different scattering factor. As the number of scatterers with a different scattering factor increased so did the asymmetry of the split peaks up to a point. Then the asymmetry would disappear again as the terrace became covered in atoms with identical scattering factors once more. It should be pointed out that the model did not allow for the shadowing of sections of the terraces by steps. If this were taken into account the asymmetry would not be expected to vanish completely after the 7 x 7 completely covered the surface. The choice of modeling regions of different scattering factor at the step edges was motivated by the observation of Osakabe et al. [39] that in the absence of contamination the 7 x 7 nucleates primarily at the upper side of step edges.

The vicinal samples were examined using two perpendicular beam incidence directions, the $[2\bar{1}\bar{1}]$ and $[0\bar{1}1]$. Incidence along the $[2\bar{1}\bar{1}]$ produced split spots and, as expected, incidence along the $[0\bar{1}1]$ did not. At incidence angles smaller than the miscut angle very poor patterns were observed for both incident directions. This was expected for the $[2\bar{1}\bar{1}]$ direction since at such small angles the steps completely shadowed the adjacent terraces from the beam. However, it came as a surprise for the $[0\bar{1}1]$ incidence direction which should be parallel to the step edges assuming that these edges were straight and ran perpendicular to the miscut direction . One explanation for this could be that the step edges form a zig-zag pattern. Phaneuf et al. [10] have previously reported the formation of an ordered array of kinks as one of two coexisting regions for Si(111) miscut towards the $[0\bar{1}1]$ direction. These they observed below a second phase transition approximately 200° C below the 7 x 7 to 1 x 1 transition. The small incidence angle patterns of our samples did not, however, improve when heated to temperatures that supported the 1 x 1 surface indicating that if kinked steps were the cause of the poor patterns observed with $[01\bar{1}]$ incidence that the kinks still existed in some form at higher temperatures.

The surfaces examined in this study might be less expected to have kinked steps than the those studied by Phaneuf and Williams since the miscut used here results in the step edges running parallel to an edge of the 7 x 7 unit cell. However, in addition to seeing poor patterns at small angles when the incident beam was perpendicular to the miscut direction, the axis of the spot splitting was observed on several occasions to rotate slightly as the 7 x 7 reconstruction formed. A similar rotation was seen in the study of Phaneuf and Williams which they attributed to the net direction of the step edges changing locally along with the presence of compensating regions forming elsewhere to preserve the micut direction. They further reported the appearance of additional satellite spots as the kinks formed. Such additional spots where occasionally observed in the experiments described here as well.

5. SILVER GROWTH ON VICINAL SILICON (111) 7 X 7 SURFACES

Silver films were deposited onto the vicinal silicon samples to observe how the presence of the steps affected the growth. The presence or lack of oscillations might seem a logical test to be used to determine the growth mode since, given enough mobility, the silver film would be expected to grow by step flow while lower mobilities would lead to nucleation on the terraces and layer-by-layer growth. However, as mentioned earlier, incidence angles smaller than the miscut angle resulted in poor diffraction patterns. Since even on the flat samples RHEED oscillations were observed only for angles less than approximately 3° the presence of oscillations could be used as a test of the growth mode only on the sample miscut by 1.2°. Figure 5.1 shows the evolution of the peak intensity of the specular beam over time for a run where silver was deposited on a 1.2° miscut sample at 230K. The single oscillation implies that the growth of at least the first monolayer of the film is not (entirely) by step flow. This fact can be used to put an upper limit on any nonthermal mobility that silver atoms might have on silicon of 140Å, the known terrace size. Of course, the relatively large value of this number makes it of little worth as an upper limit.

The period of the oscillation in Figure 5.1 corresponds to the completion of almost two monolayers. This differs from periods that correspond to a single monolayer when oscillations were observed on the flat samples. A possible explanation for the longer period is that the film is growing partially by step flow and partially from the growth of islands. How such mixed growth can affect the period of oscillation can be

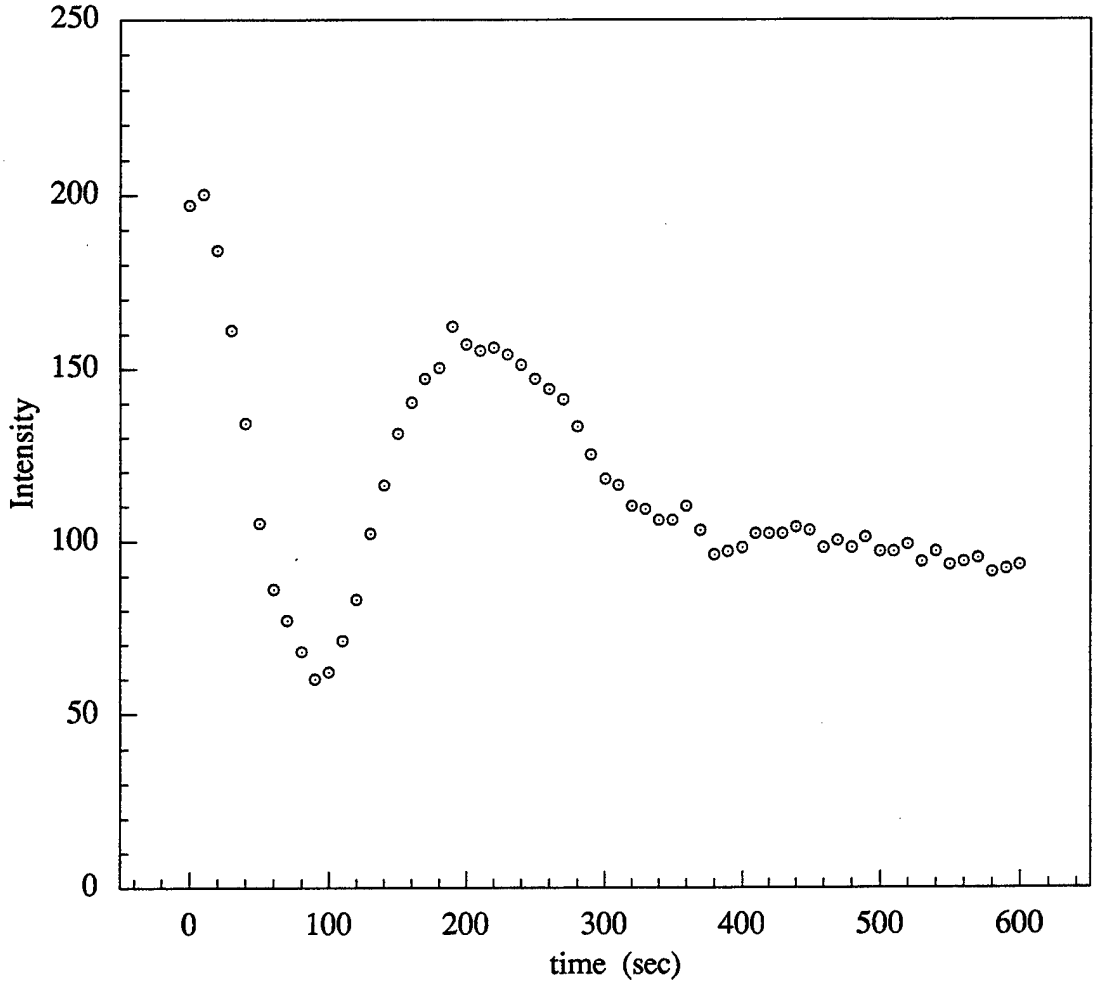

Figure 5.1 The intensity of the specular beam is shown during silver deposition onto silicon (111) miscut by 1.2° for an incidence angle of 2.4° at 230K. The period of the oscillation approximately corresponds to the completion of two monolayers

understood by considering the case where island growth is dominant, but some step flow is present. While the step flow will fill in part of a given terrace it will also fill part of the terrace below, in affect creating a surface the same size as the original terrace to be covered by that fraction of the atoms involved in island growth. Since not all the atoms are involved in island growth the period of oscillation will increase since the same number of atoms as before will be needed for the islands to reach "layer completion". It may seem that this explanation could be tested and the contributions of different growth modes sorted out by performing depositions at different temperatures. However, this will be complicated by the additional change from layer-by-layer to 3D growth as the temperature is increased.

For films grown on some samples the width of the specular spot varied with incidence direction indicating in these cases that the crystals of silver that formed were longer in a direction parallel with the step edges. Films grown at room temperature on the 2.5° miscut sample that was examined using incidence parallel to the step edges displayed a pattern that more properly was made up of wide spots instead of streaks, while the diffraction pattern of films on the sample miscut 1.2° using the same incidence direction showed streaks. This would indicate that the silver crystallites grown at room temperature have dimensions on the order of 70Å, the terrace width of the 2.5° miscut sample. This can be compared with Meyer and Rieder [40] who examined thin Ag films on the Si (111) 7 x 7 surface at 80-100K and reported islands with average diameters of about 30 Å. Low temperature deposition onto the 2.5° miscut sample again showed streaks suggesting that the island size changes with deposition temperature and that the nucleation density is more important in controlling the size of the islands than the necessity for domain boundaries to relieve strain.

Another notable observation was that no spot splitting of the silver spots was ever observed. This might indicate that silver crystallites forming on adjacent terraces are not

forming at locations differing by integral multiples of lattice vectors. Meyer and Rieder [40], using scanning tunneling microscopy, have determined that silver islands nucleate on both the faulted and unfaulted halves of the 7 x 7 reconstruction. Although these two halves of the 7 x 7 look similar they contain inequivalent sites with respect to the bulk termination. It is also possible that a splitting of the silver spots could have been obscured by streaking.

6. CONCLUSIONS

Reflection high energy electron diffraction (RHEED) was used to study the growth of silver films and the evolution of step structures on the silicon (111) surface. Silver films were deposited by molecular beam epitaxy onto the Si(111) 7 x 7 surface. Films deposited below room temperature showed RHEED intensity oscillation whose quality improved with decreasing temperature. RHEED oscillations were also improved by the application of an initial burst in the deposition flux. Such improvement and the temperature dependence of the oscillations is attributed to an increase in the island nucleation density. Oscillations observed at lower temperatures had longer periods, at least for the first oscillation, and at the in-phase condition higher final, or saturation, intensities. The separation of the silver diffraction streaks remained constant during the growth of the films. This suggests that the strain arising from the mismatch between the lattice constants of silver and silicon is relieved at domain boundaries requiring the crystallites to be of small dimension.

Vicinal silicon samples miscut from the (111) plane by 1.2°, 2.5°, and 4.5° towards the $[2\bar{1}\bar{1}]$ direction were studied. If the samples were cooled slowly through the 1 x 1 to 7 x 7 phase transition a step bunching transformation would occur that produced large (111) terraces. During this transition the diffraction spot splitting would vanish while maintaining a constant splitting width. This suggests that the transition occurs by the growth of a few terraces incorporating the others with the widths of the other terraces remaining fixed until incorporation. Diffraction spots observed on surfaces on which the

steps had been deliberately bunched were indistinguishable from flat surfaces. In this case the only way to know that the surface contained steps was the position of the shadow edge.

Silver films grown at room temperature on the 2.5° miscut sample had diffraction patterns consisting of streaks, when using beam incidence perpendicular to the step edges, but wide spots were observed when the beam was incident parallel to the step edges indicating that the silver crystallites that formed were longer in the direction parallel to the step edges. This was not observed on the sample miscut by 1.2° suggesting that the dimensions of the silver crystallites grown at room temperature were on the order of 70 Å. Low temperature deposition on the 2.5° sample also showed streaks indicating that the island nucleation density was the dominant factor in determining island size and not a necessity for domain boundaries to relieve strain. Splitting of the silver spots was never observed.

APPENDIX A: INTRODUCTION TO KINEMATIC THEORY

Although actual diffracted intensities that are measured experimentally are complicated by many factors, the kinematical approximation which neglects multiple scattering is often used to qualitatively predict the diffraction features that a surface will produce. In this approximation the intensity, I, is given by the equation

$$I(\mathbf{S}) = \left|\sum_{\mathbf{r}} f(\mathbf{r},\mathbf{S})e^{-i\mathbf{S}\cdot\mathbf{r}}\right|^2 \qquad (A.1)$$

where $\mathbf{r}$ is the summation index for the position vectors of the scatterers and $\mathbf{S}$ is the scattering vector, the difference between the outgoing, $\mathbf{k}_f$, and the incoming, $\mathbf{k}_i$, wavevectors. If equation A.1 is applied to a one dimensional line of uniformly separated scatterers the intensity will

$$I(\mathbf{S}) = \left|\sum_{m}^{N} f(\mathbf{r},\mathbf{S})e^{-ima\cdot S}\right|^2 \qquad (A.2)$$

where $\mathbf{a}$ is the lattice vector of the one dimensional lattice of N points. This equation can be transformed using the identity

$$\sum_{n=0}^{M-1} x^n = \frac{1-x^M}{1-x} \qquad (A.3)$$

to yield

$$I = \left|\frac{1-e^{-iNa\cdot S}}{1-e^{-ia\cdot S}}\right|^2 \qquad (A.4)$$

which can be rewritten in the form

$$I = \frac{\sin^2 \frac{1}{2}Na\cdot S}{\sin^2 \frac{1}{2}a\cdot S}. \qquad (A.5)$$

As can be seen in Figure A.1 which plots equation A.5 for the case where N equals 25, the intensity of this function only differs significantly from zero where $\mathbf{S}$ is an integral

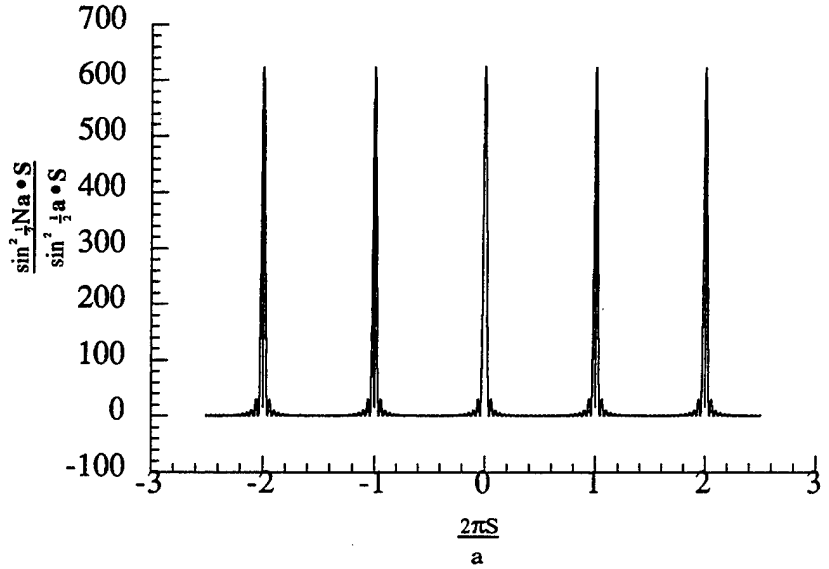

Figure A.1 Plot of equation A.5 with N=25.

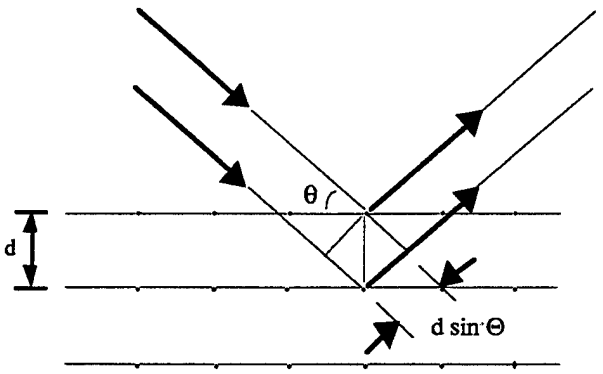

Figure A.2 Constructive interference of the specular reflections from identical, parallel planes of atoms occurs when the path difference is an integral number of wavelengths. This occurs when the Bragg condition $2d \sin \Theta = n\lambda$ is satisfied.

multiple of $\frac{2\pi}{a}$. In the more general case of a 2 or 3 dimensional lattice of scatterers this corresponds to diffraction spots occurring only when S is a reciprocal lattice vector. For a two dimensional surface of N x W scatterers the intensity is described by

$$I = \frac{\sin^2 N\mathbf{a}_1 \bullet \mathbf{S}/2}{\sin^2 \mathbf{a}_1 \bullet \mathbf{S}/2} \frac{\sin^2 W\mathbf{a}_2 \bullet \mathbf{S}/2}{\sin^2 \mathbf{a}_2 \bullet \mathbf{S}/2} \tag{A.6}$$

Equation A.5 also implies that the halfwidth of the spot is inversely proportional to N for the one dimensional case. In the two dimensional case the spot halfwidth in each direction is inversely proportional to the number of scatterers in that direction. In general for a lattice of any dimension the sharpness of the spots will increase with the number of scatterers involved.

The position of diffraction spots from bulk crystals is often described by the Bragg law,

$$2d \bullet \sin\theta = n\lambda. \tag{A.7}$$

Figure A.2 depicts how the Bragg law is derived by considering the constraints that will result in constructive interference of specular reflections from adjacent planes of atoms. The Bragg law can be shown to be equivalent to the requirement previously stated that S be a reciprocal lattice vector. Starting with the requirement for S rewritten in terms of the incident and outgoing wavevectors,

$$\mathbf{k}_f = \mathbf{k}_i + \mathbf{G}. \tag{A.8}$$

Squaring the above equation and eliminating terms gives

$$2\mathbf{k}_i \bullet \mathbf{G} = \mathbf{G}^2. \tag{A.9}$$

The spacing between adjacent hkl planes, d_{hkl}, is 2π times the inverse of the smallest reciprocal lattice vector that is perpendicular to these planes. Using this fact the above equation can be rewritten as

$$2\left(\frac{2\pi}{\lambda}\right)\left(\frac{2\pi}{d_o}\right)\sin(\theta) = \left(\frac{2\pi}{d_o}\right)^2 \tag{A.10}$$

or equivalently

$$2d_o \sin(\theta) = \lambda. \tag{A.11}$$

Since the **G** from equation A.8 is not necessarily the smallest of the reciprocal lattice vectors which are perpendicular to the planes, the d_o in equation A.10 will be the separation of adjacent planes divided by some integer which depends on **G**. When this is taken into account by multiplying the right hand side by an integer the Bragg condition is obtained.

It is often convenient to rewrite equation A.1 into other more useful forms. When the surface consists of a lattice with a multiatom basis the summations over the basis and lattice can be separated so that A.1 is rewritten as

$$I(S) = \left| \sum_{R} \sum_{j} f(\mathbf{d}_j, \mathbf{S}) e^{-iS \cdot (d_j + R)} \right|^2 \qquad (A.12)$$

where **R** is the index that sums over the lattice vectors and $\mathbf{d}_j$ is the position of the j^{th} basis atom. This equation can be further rewritten as

$$I(S) = \left| \sum_{R} e^{-iS \cdot R} F(S) \right|^2 \qquad (A.13)$$

where F(**S**) is the geometrical structure factor which is calculated only considering the basis and defined by

$$F(S) = \sum_{j} f(\mathbf{d}_j, \mathbf{S}) e^{-iS \cdot d_j} . \qquad (A.14)$$

The value of the structure factor will in general be different for different values of **S** and affect the intensity of different spots differently. In practice it is not usually possible to infer the structure factor from the observed intensites due to affects not considered in the kinematic model. However, for certain values of **S** it possible in some cases for the structure factor to be zero leading to the absence of particular spots.

When dealing with vicinal surfaces of uniform terraces containing parallel steps equation A.1 can be broken into two sums in a similar fashion as was used for the lattice with a basis. Here, the lattice points are at the step locations and the atoms on a terrace are considered as the basis. These sums are simple to compute for the case of a line of atoms with steps lacking a horizontal displacement. This leads to the equation

$$I(\mathbf{S}) = \left(\frac{\sin^2 \mathbf{ML}\bullet\mathbf{S}/2}{\sin^2 \mathbf{L}\bullet\mathbf{S}/2}\right)\left(\frac{\sin^2 \mathbf{Na}\bullet\mathbf{S}/2}{\sin^2 \mathbf{a}\bullet\mathbf{S}/2}\right) \tag{A.15}$$

assuming a unity atomic scattering factor where **L** is the primitive lattice vector for the step lattice and M and N are the total number of contributing steps and atoms per terrace respectively. The intensity from the slightly more complicated case of two dimensional terraces with each adjacent terrace having a horizontal (as well as vertical) offset from its neighbors has been calculated by Ellis and Schwoebel [41] to be described by the equation

$$\begin{aligned} I(\mathbf{S}) = {} & 16f^2\cos^2[\mathbf{S}\bullet\tfrac{1}{2}(\mathbf{a}_2+\mathbf{a}_3)]\cos^2[\mathbf{S}\bullet\tfrac{1}{2}(N\mathbf{a}_1+\mathbf{g})]\times \\ & \frac{\sin^2[\mathbf{S}\bullet\frac{1}{2}\mathbf{a}_1(N+1)]}{\sin^2(\mathbf{S}\bullet\mathbf{a}_1/2)}\frac{\sin^2[\mathbf{S}\bullet\frac{1}{2}\mathbf{a}_2(W+1)]}{\sin^2(\mathbf{S}\bullet\mathbf{a}_2)}\times \\ & \frac{\sin^2[\mathbf{S}\bullet\frac{1}{2}(N\mathbf{a}_1+\mathbf{g}_1+\mathbf{g}_2)(M+1)]}{\sin^2[\mathbf{S}\bullet(N\mathbf{a}_1+\mathbf{g}_1+\mathbf{g}_2)]} \end{aligned} \tag{A.16}$$

where $\mathbf{g} = \mathbf{g}_1 + \mathbf{g}_2 + \mathbf{g}_3$ is the vector describing the offset between terraces and there are W rows of atoms per each N width terrace.

Equation A.1 can also rewritten into a form involving the correlation function as has been done by several authors such as Lent and Cohen [42] who describe the intensity by the equation

$$I(\mathbf{S}) = \sum_{\mathbf{r}} e^{i\mathbf{S}\bullet\mathbf{r}} f(\mathbf{r}) \sum_{\mathbf{r}'} e^{-i\mathbf{S}\bullet\mathbf{r}'} f(\mathbf{r}') = N_o \sum_{\mathbf{u}} e^{-i\mathbf{S}\bullet\mathbf{u}} C(\mathbf{u}) \tag{A.17}$$

where their correlation function, C(**u**), is defined by

$$C(\mathbf{u}) = \frac{1}{N_0}\sum_{\mathbf{r}} f(\mathbf{r})f(\mathbf{r}+\mathbf{u}). \tag{A.18}$$

The correlation function is equal to the probability that two scatterers are separated by a vector **u**.

APPENDIX B: KINEMATIC SIMULATIONS

Several simulations using the kinematic approximation were performed on model surfaces. Both normal incidence with low energy electrons, as in LEED, and glancing incident angles with wavevectors corresponding to a 5 keV beam were used. The simulations using glancing angles used parameters characteristic of the RHEED apparatus and samples used for the experiments of this thesis. A series of simulations which corresponded to the initial, intermediate, and final surfaces of the step bunching transition were performed, and although the simulations used a simple stepped line model to represent the real surfaces, good qualitative agreement with the profiles from experiments was obtained.

A series of programs was written to perform these simulations. All were quite similar, and a single program for normal incidence is shown in Appendix C. Figure B.1 shows examples of the profiles that were calculated from the model surfaces. This figure demonstrates that perfect periodicity of the steps is not required to observe spot splitting. Although the profile in part (a) was calculated using an array of steps with identical spacing, the profile in part (c), which also shows splitting, was calculated from a surface which consisted of terraces of various sizes. The distribution describing the terrace sizes used to calculate part (c) was Gaussian in shape with nearly the same mean terrace size as in part (a) and had a standard deviation of approximately 3 atoms. The profiles from parts (a) and (c) were then convoluted with an instrument response function to show that such splitting would still be visible experimentally. The instrument response function was for convenience assumed to be Gaussian with a half width identical to that of a sharp spot observed experimentally from a flat, clean Si sample.

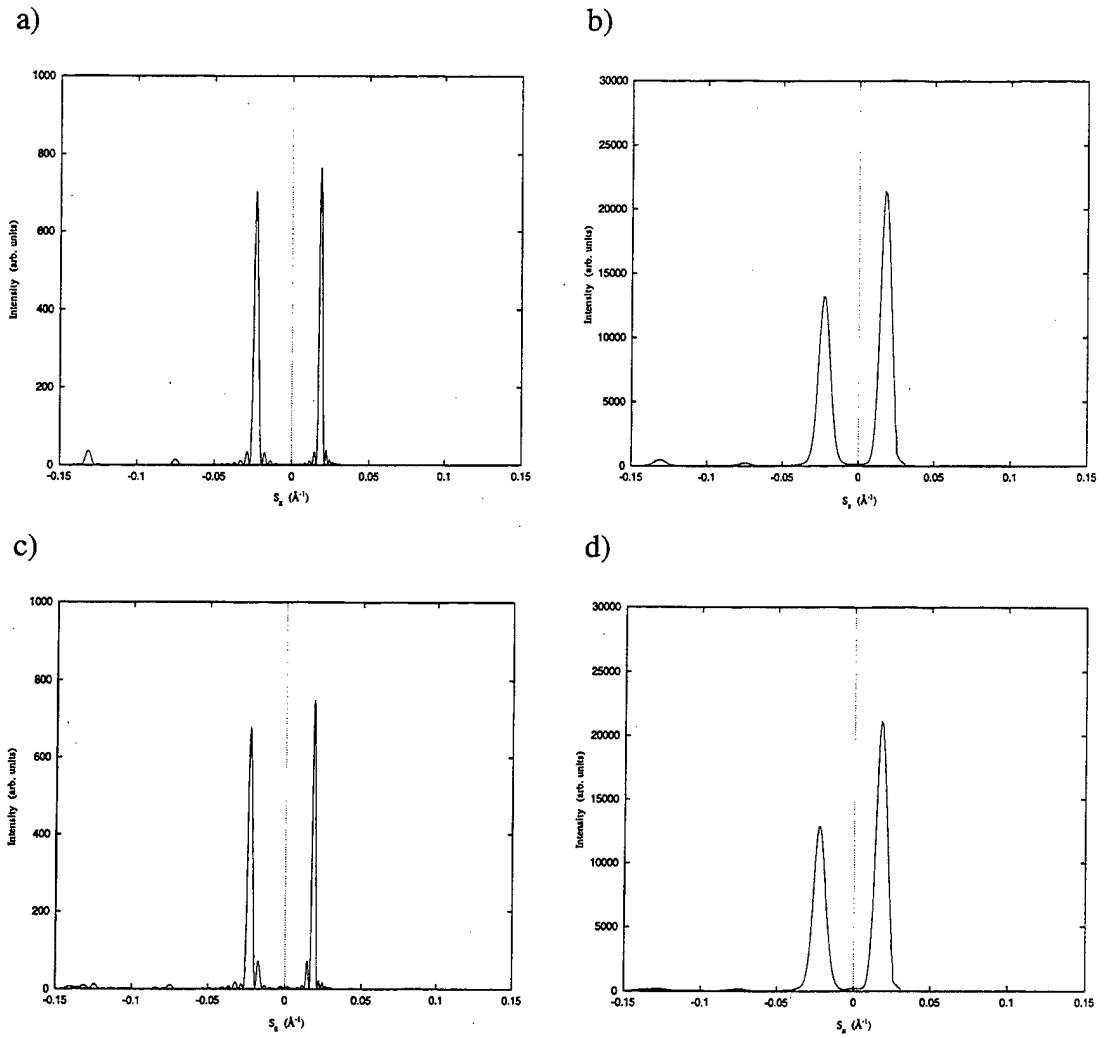

Figure B.1 Calculated profiles of the specular beam are shown for simulated surfaces using a glancing angle of 5°. In a) a surface consisting of uniform terraces corresponding to a miscut angle of 2.5° was used. Part b) shows the profile from part (a) convoluted with a Gaussian instrument response function having a FWHM of 0.008 Å^{-1} Part c) shows the profile from a surface with a Gaussian distribution of terrace sizes with approximately the same mean terrace size as used in part (a) with a standard deviation of 3 atomic lattice constants. Part d) shows the profile from part (c) convoluted with the same instrument response used for part (b).

With the exception of those in figure B.2 the simulations whose results are shown all used surfaces consisting of 300 scatterers positioned in a stepped line with 3.1 Å spacing. The step height used was also 3.1 Å corresponding to the separation of Si(111) planes. For simplicity, however, no attempt was made to model the actual bilayer surface of unreconstructed silicon or the 7 x 7 reconstruction. Since far more than 300 atoms will scatter coherently to contribute to the intensity of actual RHEED spots the number chosen for the simulation might at first seem too small. However, an examination of equation A.16 which gives the intensity from a true two dimensional surface in the kinematic approximation shows that if the other rows of atoms not modeled were included the profile would be no sharper. The affect of changing the number of scatterers included in the simulation is shown in Figure B.2 which shows simulations run on the same surface from part (c) of Figure B.1, but using 100 and 500 atoms to calculate the intensity. Any effort to compensate for the rows not modeled by adding additional atoms to the line would unrealistically sharpen the spots.

Figure B.3 shows the evolution of a spot profile during modeled step bunching using normal incidence. Part (a) shows the familiar spot splitting from a stepped surface with each spot nearly equidistant from where the unsplit specular shown in part (c) would be. The splitting is pronounced because the electron energy was chosen to be near the out-of-phase condition. In part (b) a partially bunched surface is modeled with a single large terrace and several terraces of the same width used for part (a). In (b) both the specular spot and those from the array of steps are visible.

While Figure B.3 shows the spot evolution during step bunching that would be observed at the out-of-phase condition with LEED, it is possible to observe a different profile evolution at the in-phase condition using RHEED. LEED would be insensitive to the steps at this phase condition, but because with RHEED the Ewald sphere makes a nearly parallel intersection with the lattice rods it intersects each of the step rods at a

a)

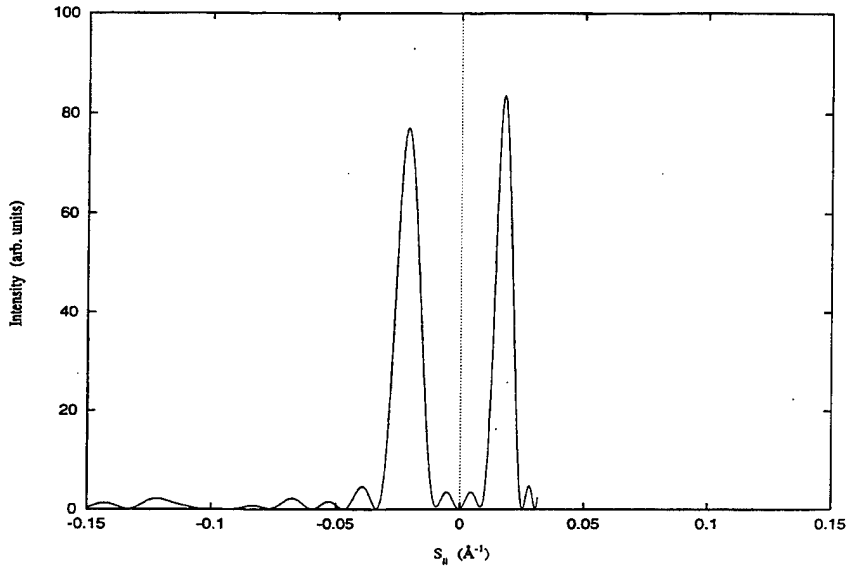

b)

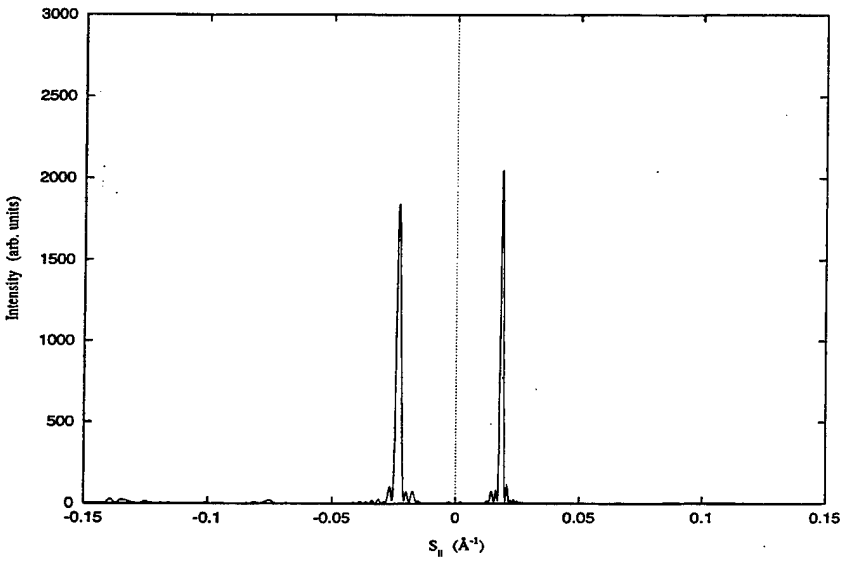

Figure B.2 a) The profile calculated from a surface with the same distribution of terrace sizes used in part (c) of Figure B.1, but using a summation over 100 scatterers is shown. b) A profile calculated using the same surface with a summation over 500 scatterers.

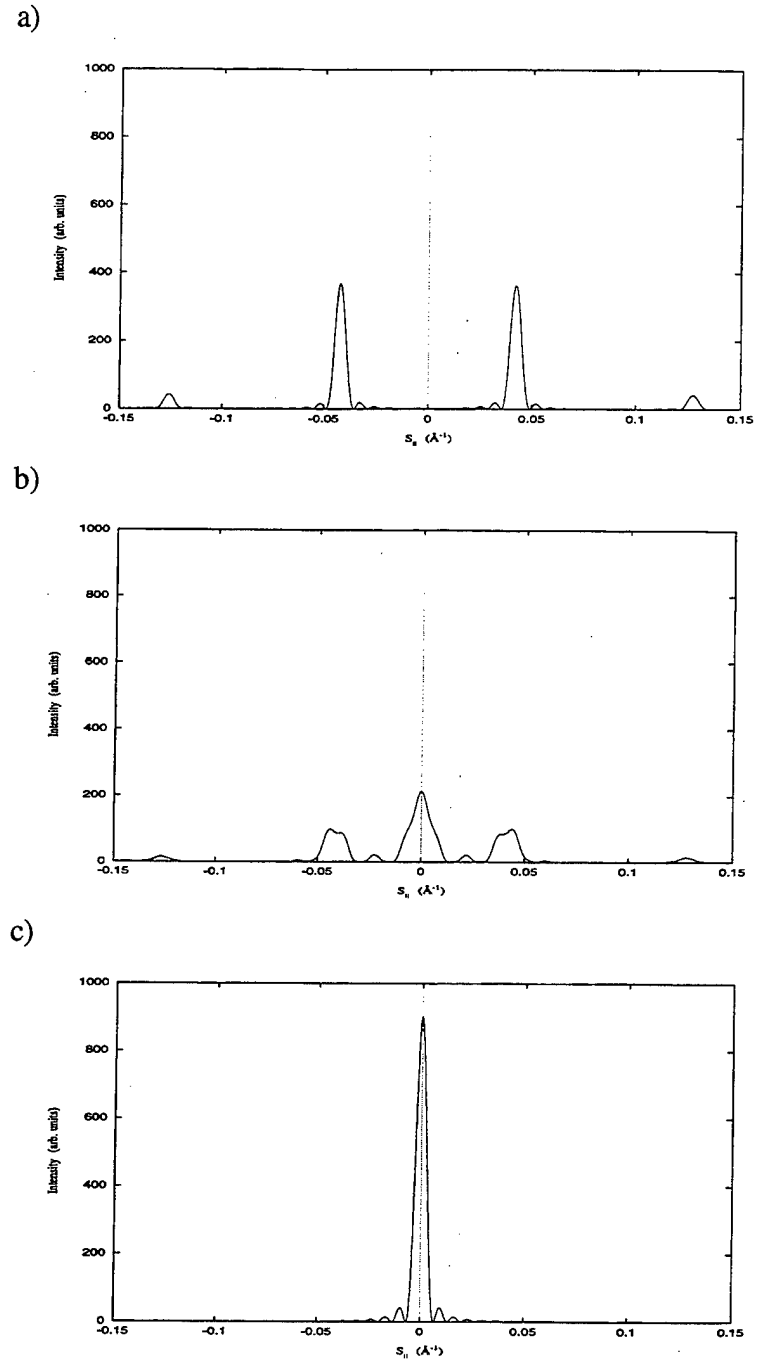

Figure B.3 Profiles calculate for normal incidence are shown. In part a) the surface used was made up of uniform terraces, in part b) the surface was half covered with a single large terrace, and for part c) the surface was flat.

different z-component of the scattering vector as shown in Figure 1.4. Figure B.4 shows the simulated evolution of a RHEED specular profile during step bunching at the in-phase condition. The specular spot is seen in all three frames, but the single spot due to a step rod diminishes as the large terrace spreads over the simulated surface. The evolution of the simulated RHEED profiles during step bunching is in qualitative agreement with the experimental observations.

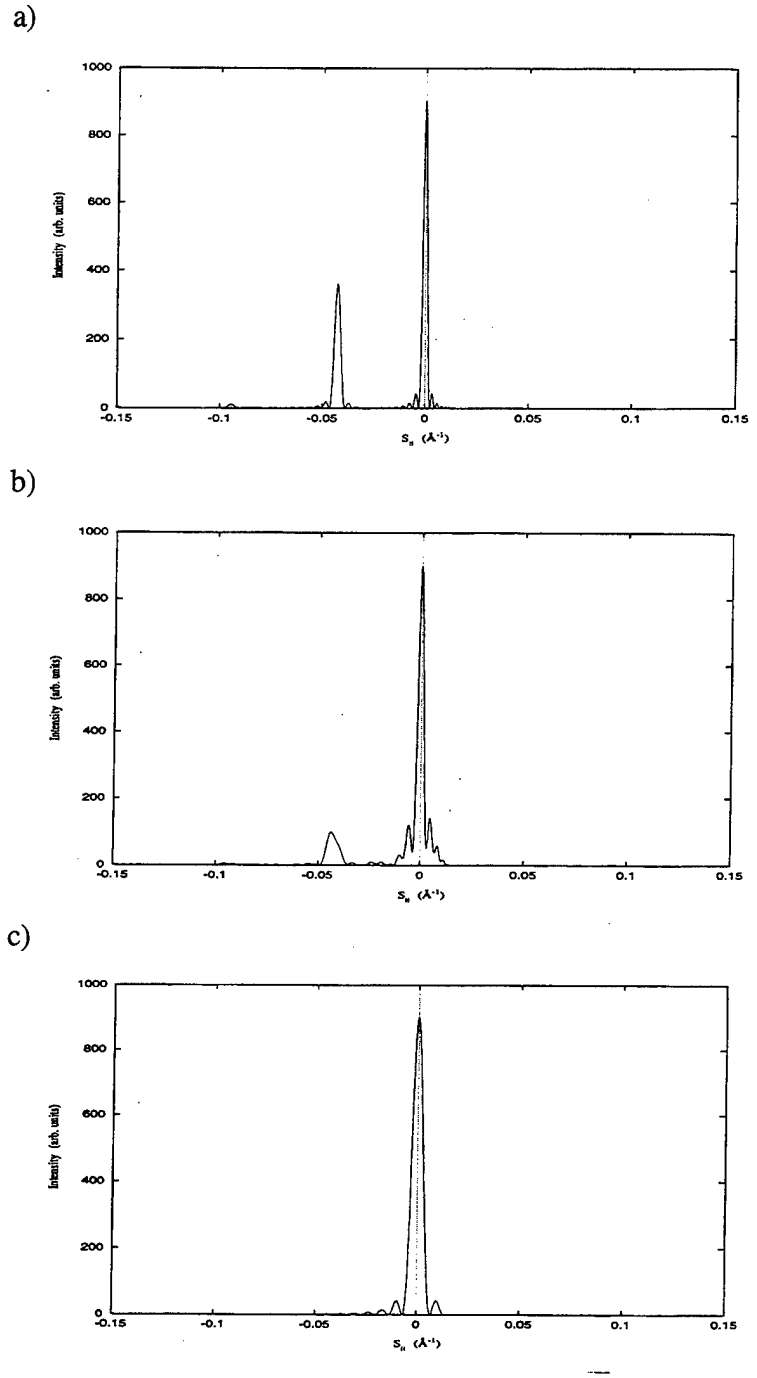

Figure B.4 The calculated specular profile at 1.6° glancing incidence is shown for a) a surface of uniform terraces corresponding to a 2.5° miscut, b) a surface which is half covered with a single large terrace and the other half covered with steps as in part (a), and c) a flat surface.

APPENDIX C: SAMPLE SIMULATION PROGRAM

```
      PROGRAM LEEDPRO
C     VERSION 1.1   03/18/97
C     PROGRAM TO MODEL SPOT PROFILES USING NORMAL INCIDENCE

      INTEGER HEIGHT (1:300), J
      DOUBLE PRECISION SPARA, SPERP, K, LSEP, RINTEN, IMINTEN
      REAL ANGLE, INTEN, PIDIV, BRACK
      PARAMETER (K=0.506)
      PARAMETER (PIDIV=0.0174532)
      PARAMETER (LSEP=3.1)

C     CALL ROUTINE TO CREATE SURFACE IN THE 1D ARRAY HEIGHT

      CALL SURF2 (HEIGHT, 300, 0.0)

      DO 500 ANGLE=70.0, 114.0, 0.005
        SPARA=K*(COS(ANGLE*PIDIV))
        SPERP=K*(1.+SIN(ANGLE*PIDIV))
        RINTEN=0.
        IMINTEN=0.
        DO 200 J=1, 300
          BRACK=SPARA*J*LSEP+SPERP*HEIGHT(J)*LSEP
          RINTEN=RINTEN+COS(BRACK)/10.
          IMINTEN=IMINTEN+SIN(BRACK)/10.
200     CONTINUE
        INTEN=RINTEN*RINTEN+IMINTEN*IMINTEN
        PRINT 250, SPARA, INTEN
250     FORMAT (1X, F11.4, 5X, F11.4)
500   CONTINUE
```

```
      END

      SUBROUTINE SURF1 (VECT, DIM, SIGMA)
C     FOR FLAT SURFACE

      REAL SIGMA
      INTEGER DIM, J
      INTEGER VECT(1:DIM)
      DO 100 J=1, DIM
        VECT(J)=1
100   CONTINUE
      END

      SUBROUTINE SURF2 (VECT, DIM, SIGMA)
C     CREATES A STEPPED SURFACE WITH A GUASSIAN TERRACE WIDTH
C     DISTRIBUTION OF STD PROPORTIONAL TO SIGMA.  THE MEAN
C     IS SET BY THE VARIABLE TER (TWICE) WITHIN THE ROUTINE.
C     THE REAL MEAN MAY BE GREATER THAN TER DUE TO ROUNDING UP

      INTEGER DIM, LEVEL, COUNT
      INTEGER VECT(1:DIM), I
      REAL SIGMA, SEED, TER
      SEED=0.33
      LEVEL=1
      COUNT=0
      TER=23.
      CALL RGAUSS (SEED, TER, SIGMA)
      DO 800 I=1, DIM
        IF (COUNT .GT. TER) THEN
          LEVEL=LEVEL+1
          COUNT=0
          TER=23.
          CALL RGAUSS (SEED, TER, SIGMA)
        ENDIF
        VECT(I)=LEVEL
```

```
        COUNT=COUNT+1
800     CONTINUE
        END

        SUBROUTINE RGAUSS (SEED, MEAN, STD)

C       SUBROUTINE TO RETURN RANDOM NUMBERS WITH A GAUSSIAN
C       DISTRIBUTION.  THE GENERATED NUMBER IS RETURNED IN THE
C       VARIABLE MEAN.  SEED SHOULD BE BETWEEN 0 AND 1.

        REAL SEED, MEAN, STD, SUM
        INTEGER I
        SUM=0.
        DO 900 I=1, 12
          SUM=SUM+RAND(SEED)
900     CONTINUE
        SUM= (SUM-6.)/12.
        MEAN=MEAN+STD*SUM
        END
```

BIBLIOGRAPHY

[1] Y. Gotoh, S. Ino, *Jap. J. Appl. Phys.* **17**, 2097, (1978)

[2] M. Jalochowski, M. Hoffmann, E. Bauer, *Phys. Rev. B* **51**, 7231, (1995)

[3] D. E. Sanders, A. E. DePristo, *Surf. Sci.* **254**, 341, (1991)

[4] W. F. Egelhoff, Jr., I. Jacob, *Phys. Rev. L ett.* **62**, 921, (1989)

[5] J. W. Evans, D. E. Sanders, P. A. Thiel, A. E. DePristo, *Phys. Rev. B* **41**, 5410, (1990)

[6] J. A. Venebles, G. D. T. Spiller, M. Hanbucken, *Rep. Prog. Phys.* **47**, 399, (1984)

[7] J. A. Venables in: *Microstructural Evolution of Thin Films*, eds. H. A. Atwater, C. Thompson (Academic Press, 1992)

[8] K. R. Roos , M. C. Tringides, *Surf. Sci.* **302**, 37, (1994)

[9] G. W. Jones, J. M. Marcanao, J. K. Nørskov, J. A. Venables, *Phys. Rev. Lett.* **65**, 3317, (1990)

[10] R. J. Phaneuf, E. D. Williams, N. C. Bartelt, *Phys. Rev. B* **38**, 1984, (1988)

[11] R. J. Phaneuf, N. C. Bartelt, E. D. Williams, W. Swiech, E. Bauer, *Phys. Rev. Lett.* **67**, 2986, (1991)

[12] R. J. Phaneuf, E. D. Williams, *Phys. Rev. Lett.* **58**, 2563, (1987)

[13] B. Z. Olshanetsky, S. A. Teys, *Surf. Sci.* **230**, 184, (1990)

[14] A. V. Latyshev, A. L. Aseev, A. B. Krasilnikov, S. I. Stenin, *Surf. Sci.* **213**, 157, (1989)

[15] A. V. Latyshev, A. B. Krasilnikov, A. L. Aseev, *Surf. Sci.* **311**, 395, (1994)

[16] E. D. Williams, E. Fu, Y.-N. Yang, D. Kandel, J. D. Weeks, *Surf. Sci.* **336**, L746, (1995)

[17] E. S. Fu, M. D. Johnson, D.-J. Liu, J. D. Weeks, E. D. Williams, *Phys. Rev. Lett.* **77**, 1091, (1996)

[18] R. J. Phaneuf, E. D. Williams, *Phys. Rev. B* **41**, 2991, (1990)

[19] F. Jentzsch, M. Henzler, *Appl. Phys. A* **46**, 119, (1988)

[20] W. Moritz in: *Reflection High-Energy Electron Diffraction and Reflection Electron Imaging of Surfaces*, eds. P. K. Larsen, P. J. Dobson (Plenum Press, 1988)

[21] M. Henzler in: *Reflection High-Energy Electron Diffraction and Reflection Electron Imaging of Surfaces*, eds. P. K. Larsen, P. J. Dobson (Plenum Press, 1988)

[22] B. S. Swartzentruber, Y.-W. Mo, M. B. Webb, M. G. Lagally, *J. Vac. Sci. Tech. A* **7(4)**, 2901, (1989)

[23] J. Yuhara, M. Inoue, K. Morita, *J. Vac. Sci. Tech. A* **11**, 2714, (1993)

[24] Y. Gotoh, S. Ino, *Thin Solid Films* **109**, 255, (1983)

[25] G. Meyer, K. H. Rieder, *Appl. Phys. Lett.* **64**, 3560, (1994)

[26] D. Bolmont, P. Chen, C. A. Sebenne, F. Proix, *Phys. Rev. B* **24**, 4552, (1981)

[27] R. J. Wilson, S. Chiang, *Phys. Rev. Lett.* **58**, 369, (1987)

[28] J.-K. Zuo, J. F. Wendelken, *Phys. Rev. Lett.* **66**, 2227, (1991)

[29] G. Raynerd, T. N. Doust, J. A. Venables, *Surf. Sci.* **261**, 251, (1992)

[30] K. R. Kimberlin, M. C. Tringides, *J. Vac. Sci. Tech. A*, **13(2)**, 462, (1995)

[31] H. A. van der Vegt, H. M. van Pinxteren, M. Lohmeier, E. Vlieg, J. M. C. Thornton *Phys. Rev. Lett.* **68**, 3335 (1992)

[32] J. Vrijmoeth, H. A. van der Vegt, E. Vlieg, R. J. Behm, *Phys. Rev. Lett.* **72**, 3843, (1994)

[33] G. Rosenfeld, R. Servaty, C. Teichert, B. Poelsema, G. Comsa, *Phys. Rev. Lett.* **71**, (1993)

[34] Z. Mitra, A. Daniluk, *Surf. Sci.* **277**, 229, (1992)

[35] Y. Horio, A. Ichimiya, *Surf. Sci.* **298**, 261, (1993)

[36] Y. Suzuki, H. Kikuchi, N. Koshizuka, *Jap. J. Appl. Phys.* **27**, L1175, (1988)

[37] S. Clarke, D. D. Vvendensky, *J. Appl. Phys.* **63**, 2272, (1988)

[38] R. S. Becker, J. A. Golovchenko, E. G. McRae, B. S. Swartzentruber, *Phys. Rev. Lett.* **55**, 2028, (1985)

[39] N. Osakabe, Y. Tanishiro, L. Yagi, G. Honjo, *Surf. Sci.* **109**, 353, (1981)

[40] G. Meyer, K. H. Rieder, *Surf. Sci.* **331**, 600, (1995)

[41] W. P. Ellis, R. L. Schwoebel, *Surf. Sci.* **11**, 82, (1968)

[42] C. S. Lent, P. I. Cohen, *Surf. Sci.* **139**, 121, (1984)

Report Number (14) IS-T--1836

Publ. Date (11) 19980223

Sponsor Code (18) DOE/ER, XF

UC Category (19) UC-400, DOE/ER

DOE